The brain and inner ear of the early Paleocene 'condylarth' Carsioptychus coarctatus: implications for early placental mammal neurosensory biology and behavior

The brain and inner ear of the early Paleocene 'condylarth' *Carsioptychus coarctatus*: implications for early placental mammal neurosensory biology and behavior

Joe Cameron[1], Sarah L. Shelley[1], Thomas E. Williamson[2], and Stephen L. Brusatte[1,2*]

[1]School of GeoSciences, University of Edinburgh, Grant Institute, James Hutton Road, Edinburgh EH9 3FE, Scotland, United Kingdom

[2]New Mexico Museum of Natural History and Science, 1801 Mountain Road, NW, Albuquerque, NM 87104-1375, USA

RUNNING TITLE: NEUROSENSORY ANATOMY OF EARLY PLACENTAL MAMMAL

*Correspondence to: Stephen L. Brusatte, School of GeoSciences, University of Edinburgh, Grant Institute, James Hutton Road, Edinburgh EH9 3FE, Scotland, United Kingdom. Telephone: +44 01316506039, E-mail: Stephen.Brusatte@ed.ac.uk

Grant sponsors: Royal Society Research Grant (RG130018), Marie Curie Career Integration Grant (630652), funding from the European Research Council (ERC) under the European Union's Horizon 2020 research and innovation programme (grant agreement No 756226, ERC Starting Grant: PalM), University of Edinburgh School of GeoSciences, National Science Foundation (EAR-1325544; DEB 1654952), Natural Environment Research Council studentship to S.S., Bureau of Land Management to TEW and SLB.

ABSTRACT: Mammals underwent a profound diversification after the end-Cretaceous mass extinction, with placentals rapidly expanding in body size and diversity to fill new niches vacated by dinosaurs. Little is known, however, about the brains and senses of these earliest placentals, and how neurosensory features may have promoted their survival and diversification. We here use computed tomography (CT) to describe the brain, inner ear, sinuses, and endocranial nerves and vessels of *Carsioptychus coarctatus*, a periptychid 'condylarth' that was among the first placentals to blossom during the few million years after the extinction, in the Paleocene. *Carsioptychus* has a generally primitive brain and inner ear that is similar to the inferred ancestral eutherian/placental condition. Notable 'primitive' features include the large, anteriorly expanded, and conjoined olfactory bulbs, proportionally small neocortex, lissencephalic cerebrum, and large hindbrain compared to the cerebrum. An encephalization quotient (EQ) cannot be confidently calculated because of specimen crushing but was likely very small, and comparisons with other extinct placentals reveal that many Paleocene 'archaic' mammals had EQ values below the hallmark threshold of modern placentals but within the zone of non-mammalian cynodonts, indicative of small brains and low intelligence. *Carsioptychus* did, however, have a 'conventional' hearing range for a placental, but was not particularly agile, with semicircular canal dimensions similar to modern pigs. This information fleshes out the biology of a keystone Paleocene 'archaic' placental, but more comparative work is needed to test hypotheses of how neurosensory evolution was related to the placental radiation.

Key words: mammal, placental, sensory evolution, neuroanatomy, CT scanning, end-Cretaceous extinction

The end-Cretaceous extinction, 66 million years ago, was a pivotal event in mammalian history. The first placentals—species, like humans, that give live-birth to well-developed young—probably originated during the Late Cretaceous, but then rapidly diversified to fill new niches in the ensuing Paleocene, after the non-avian dinosaurs went extinct (e.g., Murphy et al., 2001; Meredith et al., 2011; dos Reis et al., 2012, 2014; Liu et al., 2017). Studies have shown that mammalian taxonomic diversity, body size, morphological disparity, and evolutionary rates increased after the extinction of the non-avian dinosaurs (e.g., Alroy, 1999; Slater, 2013; Grossnickle and Newham, 2016; Halliday and Goswami, 2016a,b; Halliday et al., 2016), but nonetheless, many questions remain about the timing, pace, and drivers of the placental radiation (e.g., Archibald and Deutschman, 2001; Goswami, 2012; O'Leary et al., 2013).

Certain biological attributes of placental mammals may have aided their survival during the end-Cretaceous extinction and/or promoted their diversification in the aftermath (e.g., Wilson, 2013). Recent work has focused on life history traits such as nocturnal vs. diurnal activity patterns (Wu et al., 2017; Maor et al., 2017). Much less attention has focused on neurosensory systems. Modern mammals have the proportionally largest brains relative to body size of any vertebrates, and a novel elaboration of the forebrain called the neocortex, which imparts heightened intelligence, memory, and senses (e.g., Jerison, 1973; Nieuwenhuys et al., 1998). It is now well understood that this basic neurosensory bauplan was established early in mammalian history, in Triassic and Jurassic taxa on the stem lineage towards crown mammals (Rowe, 1996; Rowe et al., 2011). Similarly, other studies have identified major elaborations to this bauplan during the early evolution of modern placental orders such as artiodactyls, rodents, and primates, most notably increases in encephalization and the size of the neocortex (e.g., Silcox et al., 2009b; Orliac and Gilissen, 2012; Bertrand et

al., 2016). However, comparatively little is known about the brains and senses of the oldest placentals.

This gap in our knowledge largely stems from our poor understanding of the mammals that prospered during the first ca. 10 million years after the end-Cretaceous extinction, in the Paleocene (e.g., Williamson, 1996; Rose, 2006). There is a great diversity of these mammals, many of which likely belong to early-diverging placental subgroups, but much about their anatomy, phylogenetic relationships, and biology remains mysterious. Many of them are so-called 'archaic' species, which were clearly larger and more diverse than their Cretaceous forebears, but whose relationships to the modern placental orders are contentious (see review in Rose, 2006). Perhaps the most notorious of these 'archaic' placentals are the 'condylarths', a nebulous assemblage of hundreds of species that were prevalent during the Paleocene and Eocene. They are often considered to be primitive ungulate-like mammals, and probably include the ancestors of modern perissodactyls and artiodactyls (e.g., Prothero et al., 1988; Rose, 2006).

'Condylarths' are therefore pivotal for understanding the evolution of the earliest placentals after the dinosaur extinction. But, although they are represented by a rich fossil record, there has been scant work on their neurosensory biology. Over the last few years, some studies have used computed tomography (CT) to reconstruct the brains and sense organs of the 'condylarth' *Hyopsodus* (Orliac et al., 2012a; Ravel and Orliac, 2015), and other Paleocene 'archaic' mammals (e.g., Muizon et al., 2015; Orliac and O'Leary, 2016; Napoli et al. 2017), which gives insight into their intelligence and sensory abilities. However, similar studies on other key 'condylarths' are needed, particularly exemplars of the major 'condylarth' subgroups, in order to gauge variation among the earliest placentals and better test hypotheses of how their neurosensory biology was related to extinction and survivorship.

Here, for the first time, we use CT data to describe the brain, inner ear, sinuses, and endocranial nerves and vessels of a periptychid. Periptychidae is one of the major 'condylarth' subclades, and is recognized by a distinctive dentition and generalized terrestrial body plan (Shelley, 2017). The group diversified into ca. 45 species of small-to-medium-sized taxa in the very earliest Paleocene of North America, during the first ca. 4 million years after the end-Cretaceous extinction (Matthew, 1937; Archibald, 1998; Rose, 2006; Shelley, 2017; Shelley et al., in review). Using high-resolution X-ray CT scans, we digitally visualize and describe the internal endocranial morphology of one of the best preserved periptychid skulls, a specimen of *Carsioptychus coarctatus* (AMNH 27601). We make comparisons to other mammals, both modern and extinct, and use numerical methods to estimate the general intelligence, hearing range, and agility of *Carsioptychus*. This gives important new insight into the brains, senses, and neurosensory capabilities of some of the very first placentals to flourish after the dinosaur extinction.

Institutional abbreviations—**AMNH**, American Museum of Natural History, New York, New York, USA; **YPM**, Peabody Museum of Natural History, Yale University, New Haven, Connecticut, USA.

MATERIALS AND METHODS

Fossil Specimen

This study is based on part of AMNH 27601, a moderately complete cranium of the periptychid 'condylarth' mammal *Carsioptychus coarctatus* (Fig. 1). The specimen, which consists of a partial skull and associated hind limb, was collected by George Gaylord Simpson in 1929 from the Nacimineto Formation at Barrel Springs Arroyo in what is now the

Bisti/De-na-zin Wilderness area of the San Juan Basin, New Mexico, USA (Simpson, 1936a). The specimen is from either the lower or the upper fossil horizon (fossil zone A or B: Williamson, 1996, fig. 18) and so is either middle or late Puercan (Pu2 or Pu3) in age (Lofgren et al., 2004). Some portions of the cranium are missing, notably the facial region where only a few fragments of bone remain; this region has been reconstructed on the specimen. However, most of the upper teeth are preserved in situ, and the posterior portion of the cranium (from which the endocast and inner ear data were extracted) is largely complete and well preserved in three dimensions. The specimen has been compressed dorsoventrally, and in some places laterally, which has broken and distorted some of the bones. This distortion affects the shape of the extracted endocast, particularly its anterior and middle regions. The distortion is less extreme posteriorly, and has not significantly affected the size, shape, or position of the inner ear endocast.

Carsioptychus coarctatus was first described by Cope (1883), who at that time recognized it as a species of *Periptychus* given its enlarged premolar dentition with distinctive crenulated enamel. Cope (1883) observed that the specimen he was describing differed from *Periptychus carinidens* in the construction of the lingual shoulder of the premolars (lingually expanded in *Carsioptychus* compared to *Periptychus*) and in lacking a small 7th cuspule (=obliconid) on the lower molars; however, he did not consider these features sufficient to warrant generic rank for the new specimen. Matthew (1937) proposed the subgenus *Plagioptychus* in his monograph on Paleocene mammals of New Mexico, published posthumously. Simpson (1936a), citing unpublished notes of Matthew, raised *Plagioptychus* to generic rank, given that it appeared more distinct from *Periptychus* than any of the other alleged *Periptychus* species. However, *Plagioptychus* was occupied so Simpson (1936b) then proposed the name *Carsioptychus* (see Addendum by the editors, Matthew, 1937, p. 365). Much later, Van Valen (1978) also asserted that *Carsioptychus* should be

treated as a subgenus of *Periptychus*. More recently, however, some authors have concluded that there are enough morphological differences between *Carsioptychus* and *Periptychus* to warrant generic distinction (e.g., Archibald et al., 1987). This is the taxonomy that we follow here.

Computed Tomography and Visualization

The specimen was scanned by Dr. Hong-yu Yi with a GE phoenix v|tome|x micro-CT scanner at the AMNH Microscopy and Imaging Facility. It was scanned under the following parameters: voltage of 170 kV, current of 170 μA, voxel size of 69.74 μm. The resulting dataset of tiff image slices was imported into Mimics 19.0 (Materialize N.V. 2014) at the University of Edinburgh School of GeoSciences, for segmentation and three-dimensional reconstruction. The entire dataset with the full cranium was imported at 60% resolution to create a manageable file size for the endocast model. A small selection of slices from the dataset, which included the petrosals, was then imported at a resolution of 100% to create the models of the inner ears. This work was carried out by JC, under the guidance of SLS and SLB.

Standard linear, angular, and curvature measurements of the endocast, inner ear, and associated structures were made using the measuring tools in Mimics 19.0. We imported the 3D models into MeshLab 2016.12 to take volumetric measurements. Inner ear measurements were taken using the protocol of Ekdale (2013), except for cochlear coiling, which followed the protocol of West (1985).

Paleobiological Calculations

We used measurements from the endocast to calculate two paleobiological metrics for *Carsioptychus*: locomotor agility; and hearing range. There are multiple ways to calculate each metric, and the merits of different approaches have frequently been debated in the literature. To be conservative, we used multiple equations for each metric, which provide an envelope of uncertainty. The equations we used, and their sources, are provided in Table 1. For comparative purposes, the agility and hearing range metrics were also calculated for a range of Mesozoic, early Cenozoic, and extant taxa for which inner ear measurements were available (see below).

The locomotor agility scores are based on equations presented by Silcox et al. (2009a), and use the radius of curvature of the semicircular canals to calculate a general metric of agility, which ranges from 1 (sluggish) to 6 (agile/quick moving). This agility metric is based on the work of Spoor et al. (2007), who studied a range of modern species and scored their agility on this 1-to-6 scale. These equations utilize measurements of the semicircular canals, as they are part of the vestibular apparatus, which maintains balance (specifically, rotation of the head). The canals hold endolymph fluid, which accelerates when an animal moves, and is then detected by the brain and used to coordinate balance during locomotion and stabilization of the head and eyes (e.g., Schwartz and Tomlinson, 1994; Spoor et al., 2002, 2007; Malinzak et al., 2012). The size of the canals—particularly the length of their arc—affects the travel distance of the endolymph fluid, and thus the sensitivity to head movements (e.g., Oman et al., 1987; Muller, 1994). Greater sensitivity—and thus, in general, a greater arc radius—is required for faster and more agile animals that utilize rapid head movements and undergo greater changes in velocity. Positive correlations between the arc radius of the canals and agility are well established in modern mammals (e.g., Spoor and Zonneveld, 1998; Spoor et al, 2007).

Hearing range estimates (low-frequency to high-frequency range) are based on two sets of equations. The first, presented by Rosowski (1992) utilizes the cochlear basilar membrane length; the second, presented by West (1985) utilizes both the cochlear basilar membrane length and the number of cochlear turns. These equations follow from basic auditory physics. Auditory signals are detected within the cochlea, as sound vibrations of the stapes are transmitted through the endolymphatic and perilymphatic fluids of the cochlea, which disturb the basilar membrane within the cochlear cavity, sending sensory data to the brain (Meng and Fox, 1995; Ekdale, 2016). These vibrations in the fluids affect different regions of the basilar membrane depending on their frequencies. Lower frequencies are detected in the apical turns of the cochlea, meaning that lengthening the cochlea increases the sensitivity to these low-frequencies (Ekdale, 2016). Thus, Rosowski (1992) used basilar membrane length to determine hearing frequency range, and West (1985) used basilar membrane length in conjunction with the number of cochlear turns (which may enhance low-frequency detection due to changes in the spread of pressure across the basilar membrane with increased coiling [Meng and Fox, 1995; Ekdale, 2016]).

The agility equations require a measure of body mass. This is difficult for extinct species like *Carsioptychus*, whose phylogenetic positions are contentious and whose body proportions differ from those of extant groups. Mass estimates based on long bone circumference are substantially more accurate than those based on other skeletal measurements (Campione and Evans, 2012), but there is unfortunately no postcranial material associated with the skull AMNH 27601. Furthermore, most widely used equations that predict body mass based on dental measurements utilize length and width measurements of the lower molars, which are also not preserved in AMNH 27601 (see review in Shelley, 2017). Therefore, we took measurements of the lower molars from other specimens of *Carsioptychus coarctatus*, applied the m1 regression equation of Legendre (1989), and then

took the average result as a proxy for the body mass of AMNH 27601 (Table 2). We then used this average value in the agility equations. For this reason, the agility metrics for AMNH 27601 should be treated cautiously.

It is standard in fossil endocast studies to calculate the encephalization quotient (EQ), a general measure of intelligence based on relative brain size. It is calculated as the ratio of actual brain size to the expected brain size for a given body size, with 1.0 representing the average (Jerison 1973). The extreme crushing of the anterior and middle portions of the endocasts makes it difficult to determine an accurate volume measurement, which makes calculating EQ problematic. Thus, we do not provide an explicit EQ value for the specimen, but note that the EQ would have likely been small relative to most modern mammals based on the size of the well-preserved portions of the brain (see discussion below).

Comparative Material

In describing the endocast of *Carsioptychus coarctatus*, we make comparisons to several other mammals, modern and extinct. We made our most detailed comparisons to a number of other Paleogene mammals that have recently been well described from CT data. For the cranial endocast, these include: *Alcidedorbignya inopinata* (Muizon et al., 2015), a pantodont from the Tiupampan South American Land Mammal Age (Gelfo et al., 2009), possibly correlative with the late Puercan or early Torrejonian of North America (Gelfo et al., 2009; Muizon et al., 2015); and *Hyopsodus lepidus* (Orliac et al., 2012a), a smaller 'condylarth' from the Eocene. For the inner ears, these include: *Hyopsodus* (Ravel and Orliac, 2014) and *Protungulatum* sp. (Orliac and O'Leary, 2016), widely thought to be closely positioned to the base of Placentalia (although whether *Protungulatum* itself is a placental mammal is debatable: Wible et al., 2007; Wible et al., 2009; O'Leary et al., 2013).

DESCRIPTION

Overall Endocast Morphology

Our CT-based reconstruction of the cranial endocast, inner ear endocast (endosseous labyrinth and cochlea), and associated nerves, vessels, and sinuses of *Carsioptychus coarctatus* (AMNH 27601) is shown in Figures 2-3. Two-dimensional slices of the endocast and other internal structures are shown in Figure 4. The reconstructed endocast consists of both olfactory bulbs and cerebral hemispheres, the midbrain and most of the cerebellum, and the paraflocculus and most of the inner ear and surrounding sinuses on both sides. Measurements of important features are listed in Table 3. It is important to note that the specimen was somewhat deformed during fossilization: it was dorsoventrally crushed, the sphenoid complex was moved somewhat anteriorly, and the dorsal part of the rostrum was destroyed. Thus, some measurements (particularly volumes) may not be highly accurate. Similarly, some of the morphological features of the endocast may be distorted from their true shape.

The endocast is 69.45 mm long anteroposteriorly, with the forebrain region accounting for approximately two thirds of this length. When viewed in situ within the cranium (Fig. 2), the anterior limit of the endocast reaches slightly past the midpoint of the orbits, illustrating the generally small size of the brain relative to the cranium. At maximum, the endocast is 34.69 mm wide mediolaterally. The endocast does not exhibit any flexure; however, this could be an artefact of preservation.

The volume of the endocast, as preserved, is 7876 mm^3. This value, however, is likely a severe underestimate due to the dorsoventral crushing of the endocranial region. It should

be considered as a minimum value, and not an appropriate value for calculating EQ (see above). In general, the small size of the preserved brain relative to the cranium suggests—but does not conclusively demonstrate—that *Carsioptychus* may have had a low EQ score compared to modern mammals, and even other Paleocene mammals (Table 4). If true, this would suggest that *Carsioptychus* was an animal of limited intelligence, at least compared to most modern placental mammals and maybe some of its contemporaries. The exact EQ, however, can only be calculated if better specimens are eventually discovered.

Forebrain region

The mammalian forebrain is comprised of the diencephalon, which includes the thalamus, hypothalamus and pituitary, and the telencephalon, which includes the cerebral cortex, limbic system and olfactory cortex. For *Carsioptychus*, our CT scans allow us to describe the olfactory cortex and cerebral hemispheres of the telencephalon.

The olfactory bulbs form the anterior-most structure of the forebrain region (Fig. 3, ob). On the *Carsioptychus* endocast, the left olfactory bulb cast is nearly complete and only moderately distorted; however, the right bulb cast is deformed due to dorsoventral crushing of the braincase (Figs. 2-3). The olfactory bulbs of *Carsioptychus* are large and ovoid, anteroposteriorly longer than mediolaterally wide. Within the cranial cavity, the bulbs are mediolaterally expanded to fill the entire interorbital distance. The width to length ratio of the left bulb is 0.5, with the length accounting for 30% of the total length of the endocast. The olfactory bulbs of *Carsioptychus* are more elongate than those in *Alcidedorbignya* (where the width to length ratios of the left and right bulb are 0.63 and 0.58, respectively, and the length comprises 26% of the total endocast length; Muizon et al., 2015) and *Hyopsodus* (width to

length ratios of the left and right bulb are 0.60 and 0.63, respectively, and comprise 23% of the total length of the endocast; Orliac et al., 2012a).

In *Carsioptychus,* the left and right bulbs are joined along their length, with a subtle median sulcus defining the two bulbs anteroposteriorly in dorsal view (Fig. 3C-D). The bulbs do not appear to diverge and separate from one another anteriorly. On the ventral surface, there is a sulcus extending from the anteroexternal edge of each bulb, posteromedially towards the circular fissure (best observed on the left side of the endocast). This sulcus delimits the olfactory bulb from the accessory bulb cast. A small canal cast extends anteriorly out of the accessory bulb cast: on the left bulb this canal is deflected medially, and on the right one it is deflected laterally due to distortion of the specimen. We interpret these canals as casts of the nerves associated with the vomeronasal organ (Fig. 3, vnn; Fig. 4, vcc). The presence of accessory olfactory bulbs and an associated vomeronasal organ is widespread across Mammalia (Taniguchi et al., 2011). Accessory olfactory bulbs are present in the Early Cretaceous basal dryolestid *Vincelestes* (Averianov et al., 2013; Macrini et al., 2007) but have not been reconstructed in any other Paleocene taxa at present.

Posteriorly, the olfactory bulbs of *Carsioptychus* are separated from the cerebral hemispheres by the circular fissure, so that the cerebral hemispheres do not overlap the olfactory bulbs. The circular fissure is shallow and short anteroposteriorly, and is barely differentiated from the posterior border of the olfactory bulbs region. This morphology is present in *Vincelestes* (Macrini et al., 2007) and widely observed in other Paleocene taxa such as *Alcidedorbignya* (Muizon et al., 2015), *Paramys* (Bertrand et al., 2016), and *Plesiadapis* (Orliac et al., 2014), and is likely present in the primitive mammalian ancestor (Rowe et al. 2011).

Immediately posterior to the circular fissure is the cerebrum, which consists of left and right hemispheres (Fig. 3, cbh). The hemispheres are divided along the midline by a

longitudinal sulcus (Fig. 3, los). Each hemisphere is ovoid and narrows anteriorly, with a (maximum) width to length ratio of 0.42 and 0.46 for the left and right hemispheres, respectively. This is anteroposteriorly shorter and mediolaterally broader than the ratios of taxa such as *Alcidedorbignya* (0.50: Muizon et al., 2015) and *Hyopsodus* (0.65: Orliac et al., 2012a), but comparable to that of *Onychodectes* (0.45: Napoli et al., 2016). When assessing these comparisons, however, it is important to note that the *Carsioptychus* specimen is dorsoventrally crushed, which may affect its measurements. The cerebrum is restricted anteriorly so that it does not overlap the olfactory bulb region, and posteriorly so that it does not overlap the midbrain, which is widely exposed.

The cerebrum is lissencephalic, and lacks the complex array of gyri and sulci that characterize gyrencephalic taxa, with the exceptions of the longitudinal, transverse, and rhinal sulci. There is no indication of a suprasylivian or lateral sulcus. On the dorsal surface of the cerebrum, the longitudinal sulcus demarcates the path of the dorsal sagittal sinus (Evans and de Lahunta, 2012). The sulcus is shallow but fairly uniform along its length, indicating that the sinus was not deeply imbedded within the meninges (Macrini et al., 2007). The posterior border of the cerebral hemispheres is demarcated by a faintly marked transverse sulcus (Fig. 3, trs), which, in life, conveyed the transverse sinus (Evans and Lahunta, 2012).

The rhinal fissure is discernible on both sides of the endocast, positioned towards the lateral edge of the cerebrum (Fig. 3, rhf). The rhinal fissure demarcates the boundary between the dorsal and lateral pallia, separating the palaeocortex (comprising the piriform lobe) ventrally from the remainder of the telencephalon—namely the neocortex—dorsally (Butler and Hodos, 1996; Liem et al., 2001; Rowe et al., 2011; Evans and de Lahunta, 2012). On the endocast of *Carsioptychus* described here, the rhinal fissure is visible in dorsal view as a well-defined sulcus (Fig. 3C-D); however, we cannot confidently comment on its dorsoventral position due the specimen being crushed. Despite the crushing, the position of

the rhinal fissure indicates the neocortex was small and dorsoventrally restricted (Fig. 3, nc), exposing the piriform lobe ventrally (Fig. 3, pil) and the midbrain posteriorly. Due the relatively unexpanded neocortex, the piriform lobe is exposed and visible lateral to the rhinal fissure in dorsal view on the endocast, but its shape in lateral view cannot be accurately described due to dorsoventral crushing of the specimen (it was likely positioned lateroventral to the rhinal fissure in life).

The neocortex is represented by two small lobes on the dorsal surface of the endocast, separated by the longitudinal sulcus (Fig. 3, nc). The neocortex maintains a relatively constant width along its length, and does not exhibit the posterior expansion observed in some younger Paleogene taxa such as *Hyopsodus* and *Meniscotherium* (Orliac et al., 2012a). The contour of the rhinal fissure, demarcating the lateral border of the neocortex on the endocast (ventral border in life), does not inflect or deflect along its length. Inflection or deflection of the rhinal fissure would suggest delineation of neocortical lobes, and is tentatively present in younger Paleogene taxa such as *Meniscotherium* (Orliac et al., 2012a). In general, the neocortex of *Carsioptychus* is small and unexpanded relative to its enormous size in most modern placental mammals and some Paleocene mammals, but is more in line with the unexpanded neocortices of Paleocene taeniodonts (Napoli et al., 2017) and pantodonts (Muizon et al., 2015).

On the ventral surface of the endocast of *Carsioptychus* is a shallow cast of the hypophyseal fossa (Fig. 3, hyp). The fossa is mediolaterally wider than anteroposteriorly long, with a width to length ratio of 1.14, and its posterior border is demarcated by the dorsum sellae (Fig. 3E-F). The hypophyseal cast in *Carsioptychus* is positioned more anteriorly on the endocast in comparison to several other Paleogene taxa, including *Alcidedorbignya* (Muizon et al., 2015), *Hyopsodus* (Orliac et al., 2012a), and *Onychodectes* (Napoli et al., 2017), but is more similar to the condition in *Vincelestes* (Macrini et al., 2007).

Midbrain region

The mammalian midbrain comprises the tectum, tegmentum, and isthmus. Of these regions, only the tectum can be described in *Carsioptychus*. On the endocast of *Carsioptychus*, the midbrain and hindbrain are poorly defined from one another and the structures of the midbrain are poorly preserved and deformed (Fig. 3). Consequently, it is difficult to quantify the area of midbrain exposed on the dorsal surface of the endocast; however, upon visual inspection, it appears that the midbrain region of *Carsioptychus* is not as widely exposed as that observed in *Alcidedorbignya* (Muizon et al., 2015) and *Hyopsodus* (Orliac et al., 2012a). Instead, the dorsal midbrain exposure evident in *Carsioptychus* is comparable to that of *Paramys* (Bertrand et al., 2016), *Pucadelphys* (Macrini et al., 2007), and *Vincelestes* (Macrini et al., 2007). The tectum of the midbrain in *Carsioptychus* is exposed on the dorsal surface of the endocast due to the dorsal restriction of the neocortex. The inferior and superior colliculi are not discernible on the endocast, which is likely due to the poor preservation of the specimen (although it is possible that these structures genuinely did not leave an imprint on the dorsal surface of the endocast).

Hindbrain region

The mammalian hindbrain region consists of the medulla, pons, and cerebellum. On the endocast of *Carsioptychus* we are able to describe the cerebellum, which includes the vermis and paraflocculi. The hindbrain of *Carsioptychus* is poorly delimited from the midbrain but comprises approximately 22% of the total length of the endocast. The proportions of the hindbrain are comparable to both *Alcidedorbignya* (Muizon et al., 2015) and *Hyopsodus*

(Orliac et al., 2012a), where the hindbrain also comprises ca. 20% of the total endocast length.

A large swelling is positioned on the dorsal surface of the cerebellum, slightly offset to the left on the endocast (due to deformation of the specimen). As this region has been deformed, the boundaries between regions of the brain and the original shapes of structures are not always clear. However, we interpret the swelling as the cast of the cerebellar vermis (Fig. 3, ve). In dorsal view, the swelling is nearly square in shape, with a width to length ratio of 1.07. The right lateral border of the vermis exhibits a shallow sulcus, which we interpret as the right paramedian fissure. This fissure separates the vermis from the lateral lobes of the cerebellum (the right lateral lobe is faintly discernible). The posterior border of the vermis is delimited by a deep groove for the ossified tentorium cerebelli (Figs. 3-4, otc) (Evans and de Lahunta, 2012).

The paraflocculi are lobes of the cerebellum associated with coordination, balance, and vestibular sensory acquisition (Butler and Hodos, 1996). In *Carsioptychus*, the paraflocculi are represented by the casts of the subarcuate fossae on both sides of the endocast, which project laterally as distinct, but irregular conical-shaped lobes (Fig. 3, pf). The paraflocculus would have filled all or part of the subarcuate fossa. In dorsal view, the paraflocculi (=subarcuate fossae casts) are positioned immediately anterior to a mediolateral line transecting the anterior border of the vermis. The paraflocculi form the lateral-most features of the endocast, extending just beyond the piriform lobe (Fig. 3, pil). This is in contrast to morphology observed in *Alcidedorbignya* (Muizon et al., 2015) and *Hyopsodus* (Orliac et al., 2012a), in which the piriform lobe extends considerably further laterally than the paraflocculus. However, we note that the laterally prominent position of the paraflocculi in *Carsioptychus* may be a product of the dorsoventral crushing of the specimen.

Cranial nerves, vessels, and sinuses

Several cranial nerves and elements of the venous drainage system are reconstructed on the endocast of *Carsioptychus*.

On the ventral surface of the endocast, a pair of canals is present on the anterior surface of the accessory olfactory bulbs. Interpreting these canals is difficult given the distortion of the specimen and the lack of any similar canals on other Paleogene taxa. The two canals are similar to each other in both size and the position where they contact the olfactory bulbs, suggesting they are in their natural position. However, the right canal is inflected medially, while the left one is deflected laterally, indicating that there is some distortion. The canals are too large to be interpreted as the cast of the olfactory nerve (CN I), given that axons of the olfactory nerve do not form a discrete nerve trunk (Evans and de Lahunta, 2012). Instead, we tentatively interpret them as casts of one of the nerves (terminal or vomeronasal) associated with the vomeronasal (Jacobson's) organ (Evans and de Lahunta, 2012) (Fig. 3, vnn; Fig. 4, vcc). The vomeronasal organ is an auxiliary olfactory sense organ and is associated with the flehmen response (Kaverne, 1999; Evans and de Lahunta, 2012). Similar canals have not been documented for any other Paleocene taxa, but a vomeronasal organ is present in a wide variety in extant mammals, including rodents, ungulates, and carnivores (Døving and Trotier, 1998; Kaverne, 1999).

The optic chiasm is positioned immediately posterior to the circular fissure (Fig. 3, cf). The right and left optic nerve (CN II) canal casts are poorly preserved. A small canal cast is observable, with its position likely indicating that the right and left canals are confluent.

Located posterior to the optic chiasm, and on the anterior border of the hypophyseal cast, are two pairs of canal casts (Fig. 3E-F). The anteromedial-most pair is a cast of the canals which contained the oculomotor nerve (CN III), trochlear nerve (CN IV), the

ophthalmic branch of the trigeminal nerve (CN V_1), abducens nerve (CN VI), and the ophthalmic vein (Fig. 3, opb). The posterolateral-most pair is a cast of the canals which contained the maxillary branch of the trigeminal nerve (CN V_2) (Fig. 3, mxb). On the left side of the endocast, the two pairs are distinctly separate from each other, indicating that the two canals may have exited the cranium via separate foramina: the sphenorbital fissure (for CN III, IV, V_1 and VI) and foramen rotundum (for CN V_2). However, it is worth noting that these bony openings are not preserved on the cranium of the *Carsioptychus* specimen we scanned, and on the right side of the endocast the two canals seem to converge anteriorly. Thus, the condition in *Carsioptychus* is not immediately clear, although the fact that the two canals are separate on the right side and only converge far anteriorly on the left suggest that the canals may have been separate in life. The inferred primitive placental condition is a single opening for all of the aforementioned nerves, which is called the sphenorbital fissure (O'Leary et al., 2013). In most mammals, however, the ophthalmic (V_1) and maxillary (V_2) branches of the trigeminal nerve exit the cranium via separate openings—which are denoted as the foramen rotundum and sphenorbital fissure, respectively (Macrini, 2009)—but in extant artiodactyls the two branches both exit via the sphenorbital fissure (Black, 1920). In *Maiorana,* an earliest Puercan periptychid, the sphenorbital fissure and foramen rotundum are both present as discrete openings, demonstrating the separation of these two nerve tracts (YPM VPPU 014171; Muizon et al., 2015). This is also the case for *Alcidedorbignya* (Muizon et al., 2015), although in the younger *Hyopsodus* the openings appear to be confluent (Orliac et al., 2012).

In *Carsioptychus,* at the posterior end of the lateral-most canal cast (for CN V_2), there is a small posteriorly directed protuberance, which were infer as a cast of the mandibular branch of the trigeminal nerve (CN V_3) (Fig. 3, mdb). The cast of CN V_3 exits the cranium via the foramen ovale.

Casts of the facial and vestibulocochlear nerves (CN VII and VIII, respectively) are visible entering the modiolus of the cochlea. The cast of the hypoglossal nerve (CN XII) is not preserved on the endocast.

The endocast also exhibits numerous elements of the venous drainage system, including sulci for the dorsal sagittal sinus and transverse sinus (Fig. 3, trs), and canals for the sigmoid sinus (Fig. 3, sis), occipital emissary vein (Fig. 3, oev), and capsuloparietal emissary vein (Fig. 3, cev).

In lateral view, there is a complex of canals around the auditory region (Fig. 2A-D, 3A-B). The largest canal cast (best observed on the left side) is positioned dorsal to the auditory apparatus; it extends anteriorly and then ventrally to exit the cranium via the postglenoid foramen. We identify this structure as the cast of the capsuloparietal emissary vein (Wible and Hopson, 1993; Evans and de Lahunta, 2012; Muizon et al., 2015). In eutherians, this vein arises from the transverse sinus, at the point where the sinus also branches into the sigmoid sinus and superior petrosal sinus (Wible and Hopson, 1993; Evans & de Lahunta, 2012). Posteriorly, the capsuloparietal emissary vein cast is confluent with the cast for the condyloid vein (McDowell, 1958; Wible, 2008; Evans & de Lahunta, 2012) (Fig. 3, coc). On the right side of the endocast, where the condyloid canal cast arises from the transverse sinus/capsuloparietal emissary vein, a small, ventrally projecting, canal-like protuberance is present, which we tentatively identify as the sigmoid sinus (Wible and Hopson, 1993; Muizon et al., 2015). The full extent of the sigmoid sinus is not preserved on the endocast, but it likely extended ventrally to exit the cranium via the jugular foramen (Wible and Hopson, 1993; Evans and Lahunta, 2012). The superior petrosal sinus is not evident on the reconstructed endocast.

Several other canals are reconstructed, branching from the capsuloparietal emissary vein. The cast of the occipital emissary vein arises from the capsuloparietal vein cast and

extends posteriorly to exit the cranial cavity via a small foramen within the exoccipital component of the mastoid protuberance on the posterolateral corner of the braincase (Wible et al., 2004; Martínez et al., 2016). A cast of the posttemporal canal is present (Fig. 3, ptc), converging with the ventral surface of the capsuloparietal emissary vein cast and positioned anterior to the level of the auditory apparatus. In life, this canal transmitted the posterior division of the ramus superior of the stapedial artery, as well as the arteria dilpoetica magna and veina diploetica magna (Wible, 2008; Muizon et al., 2015). Several other small canals are preserved more ventrally along with the capusuloparietal emissary vein. One extends anteriorly from the capsuloparietal emissary vein, to exit via the supraglenoid foramen within the squamosal, on the posterior root of the zygomatic arch (as described in several archaic mammals by Cope [1880]). Two further canals extend from the cast of the capsuloparietal emissary vein into the posterior root of the zygomatic arch, but do not appear to exit via any observable foramina. We interpret these smaller branches as sinus drains for the temporomandibular muscles (Fig. 3, sdtm).

Inner ear

The petrosals of AMNH 27601 are generally well preserved, although the tympanic surface on both sides of the cranium has been eroded such that some of the internal cavities (that housed the cochlea and semicircular canals) have been exposed. The left auditory region is better preserved than the right, and therefore the left bony labyrinth of AMNH 27601 has been reconstructed and described here (Figs. 5-6). Measurements of the cochlea and semicircular canal, and comparisons with other key taxa, are presented in Table 5. Comparisons between *Carsioptychus* and previously published inner ear endocasts of two other Paleogene ‘condylarths’, *Protungulatum* and *Hyopsodus*, are shown in Figure 7. Aside

from differences in the number of cochlear turns and cochlear length (Table 5), there are some key morphological differences between *Carsioptychus* and *Alcidedorbignya*, *Protungulatum*, and *Hyopsodus*.

Cochlear canal. The spiral cochlear canal of *Carsioptychus* is 9.27 mm long. This is longer than that of *Protungulatum* (7.1 mm), but fairly similar to that of *Hyopsodus* (10.10 mm) and *Alcidedorbignya* (8.48-10.86 mm). The cochlear canal in *Carsioptychus* turns 1.67 times, with a rotation of 600°. This is slightly greater than in *Protungulatum* (1.54 turns and rotation of 554°) and *Alcidedorbignya* (1.5 turns and 540°), but less than in *Hyopsodus* (2.25 turns and 765°). Both basal and apical turns of the cochlear canal remain separate in *Carsioptychus* (Fig. 6G-H). This is in contrast to the condition of *Protungulatum* where the apical turn contacts the basal turn, but is similar to that of *Hyopsodus* where only the apex touches the basal turn, and the same as *Alcidedorbignya* whose cochlea is loosely coiled.

The cochlea of *Carsioptychus* is trochospiral in shape (fig. 6A-B, C-D, K-L, co), with an aspect ratio of 0.70. It is similar to the spiraled cochlea and high aspect ratio (0.77) of *Hyopsodus*, but contrasts with the low spired (near planispiral) shape and low aspect ratios of *Protungulatum* (aspect ratio of 0.51) and *Alcidedorbignya* (0.40-0.48). The cochlea of *Carsioptychus* is also fairly rounded, contrasting with that of the more elliptical cochlea in *Hyopsodus*, which has an elongated anteroposterior axis. In *Carsioptychus*, the cochlea is oriented anteroposteriorly, with the plane of the spiral oriented 60° to the horizontal plane of the cranium. The angle between the cochlear basal turn and the plane of the lateral semi-circular canal is wide (29°). This is within the range of specimens of *Alcidedorbignya* (0.21°-0.35°), and substantially higher than in *Hyopsodus* (20°).

The primary bony lamina is evident as a sulcus, extending from the base of the cochlea, and becoming shallower before disappearing just short of the apex (Fig. 6 G-H, K-L,

pbl). The primary bony lamina, in conjunction with the secondary bony lamina, would have separated the scala tympani (tympanic duct) and scala vestibuli (vestibular duct) in life (Evans and deLahunta, 2012). The sulcus for the primary bony lamina appears discontinuous in places, but this is likely an artefact of preservation. The secondary bony lamina is present along the first 130^{o} of the basal turn, and is shallower than the sulcus for the primary bony lamina (Fig. 6 A-B, G-H, K-L, sbl). The distance between the two laminae thus narrows towards the apex. The primary bony lamina is similarly present in *Protungulatum*, *Hyopsodus*, and *Alcidedorbignya*. In *Hyopsodus*, the secondary bony lamina also extends for almost the same distance (135^{o}), although in *Carsioptychus* the ratio to cochlear length is greater (22% vs. 18%). However, in *Alcidedorbignya*, the secondary bony laminae is present for a much shorter length (90^{o}), whereas it extends much further in *Protungulatum* (340^{o}).

The cast of the cochlear canal tapers along its length; it is widest at its base, and decreases in size until the secondary bony lamina sulcus disappears, from which point it more gradually decreases in size towards the apex (Fig. 6 A-B, M-N). The same condition is seen in *Alcidedorbignya*, but *Hyopsodus* has a much larger change in size and shape, while the canal of *Protungulatum* is roughly constant in width, with only a very slight taper towards the apex. Casts of the facial and vestibulocochlear nerves (CN VII and VIII respectively) are present entering the modiolus of the cochlea.

Semicircular canals. Measurements of the semicircular canals are provided in Table 5. The anterior semicircular canal (ASC) of *Carsioptychus* has the largest radius of the three canals, although it is only the second longest. While the ASC similarly has the largest radius in *Protungulatum*, *Hyopsodus*, and *Alcidedorbignya*, the ASC is the longest of the canals in these taxa. The ASC of *Carsioptychus* exhibits very little bending relative to its plane (Fig. 6 C-D), and it has a near semi-circular profile in lateral view (Fig. 6 E-F), with an aspect ratio

close to one. The ASC of *Hyopsodus* and *Alcidedorbignya* also exhibit little to no bending relative to their planes, as well as grossly semi-circular shapes. The ASC of *Protungulatum* shows little bending also, but has an elliptical arc. The ASC connects with the posterior semicircular canal (PSC) at the common crus, which is 2.83 mm long and projects posterodorsally, as also seen in *Protungulatum*.

The PSC of *Carsioptychus* has the same radius as the lateral semicircular canal (LSC), and is the longest of the three canals. This differs from the condition in *Hyopsodus*, *Protungulatum*, and *Alcidedorbignya*, in which the PSC is the second longest of the canals. However, in all of these taxa, including *Carsioptychus*, the PSC has a smaller radius than the ASC (although in *Protungulatum* and *Hyopsodus* the PSC is larger than the LSC, and in *Alcidedorbignya* the PSC is smaller than the LSC). The PSC in *Carsioptychus* has a slight lateral deflection along its midsection relative to the vertical plane in lateral view (Fig. 6 E-F), and in posterior view has an elliptical shape, slightly higher dorsoventrally than wide mediolaterally (Fig. 6 M-N). This midsection deflection is also seen in *Protungulatum*, but contrasts with straight PSCs of *Hyopsodus* and *Alcidedorbignya*. The PSCs of these three comparison taxa also have largely semi-circular profiles, unlike the more elliptical arc of *Carsioptychus*. The PSC meets the LSC at a secondary common crus, where neither canal can be distinguished (Fig. 6, scc). A secondary common crus is also present in *Protungulatum, Hyopsodus,* and *Alcidedorbignya*; unlike *Carsioptychus*, in *Protungulatum* the PSC and LSC can still be distinguished.

The LSC of *Carsioptychus* is the shortest in length of the three canals, as is observed in *Protungulatum*, *Hyopsodus*, and *Alcidedorbignya*. However, its radius is equal to that of the PSC, whereas the LSC has the smallest radius of the three canals in *Protungulatum* and *Hyopsodus*, and in *Alcidedorbignya* the LSC radius is larger than that of the PSC. The LSC of *Carsioptychus* is slightly dorsally deflected relative to the horizontal plane in lateral view

(Fig. 6 E-F), and has an elliptical arc. This elliptical shape is seen also in *Protungulatum* and *Hyopsodus*, although *Alcidedorbignya* has a semi-circular profile. *Protungulatum* also has a similar slight dorsal bend in the LSC, while *Hyopsodus* exhibits a ventral bend, and in *Alcidedorbignya* the LSC remains straight along its plane.

The angle between the planes of the ASC and LSC is the smallest of the inter-canal angles in *Carsioptychus*, whereas the angle between the ASC and PSC is the largest. The ASC/LSC angle is also the smallest in *Protungulatum*, but it is the largest in *Hyopsodus*, whose smallest angle between planes is that of the ASC/PSC. The largest angle between planes of *Protungulatum* is the LSC/PSC angle, as also appears to be the case for *Alcidedorbignya* from the ranges given by different specimens. The smallest angle in *Alcidedorbignya* is between the ASC and PSC. The ASC of *Carsioptychus* constitutes the dorsal-most extent of the semi-circular canals, as it extends slightly above the PSC in lateral and medial views. This is also seen in *Protungulatum* and *Hyopsodus*, although in *Alcidedorbignya* the PSC extends to roughly the same point as the ASC.

The three canals of *Carsioptychus* attach to the vestibule via ampullae. These are all strongly inflated, with the anterior ampulla slightly more inflated than the other two (Fig. 6, aa). The anterior ampulla attaches to the vestibule just above the plane of the LSC, the posterior ampulla immediately below this plane, and the lateral ampulla level with this plane (Fig. 6 E-F). The ampullae of *Protungulatum*, *Hyopsodus* and *Alcidedorbignya* are all relatively similar to this morphology, although in *Hyopsodus* the lateral ampulla sits just below (rather than level with) the LSC plane, and the lateral ampulla of *Alcidedorbignya* is more of an inflation of the secondary common crus than a discrete ampulla.

The vestibular aqueduct of *Carsioptychus* is visible in the left inner ear; it originates immediately anterior to the base of the common crus and extends posteromedially to the external aperture, which is level with the apex of the common crus (Fig. 6, va). It slightly

curves at its midsection to extend laterally (Fig. 6 E-F). The vestibular aqueduct is also present in the inner ear models of *Protungulatum* and *Alcidedorbignya*, and in these taxa the aqueducts have similar origins to *Carsioptychus* in relation to the common crus, although in both cases the aqueduct is shorter than that of *Carsioptychus*.

STATISTICAL ANALYSES

Hearing Range

Based on the equations of Rosowski (1992), the hearing range of *Carsioptychus* at 60 dB was between 58.91kHz and 0.90kHz. Using the equations of West (1985), at 60 dB the range was 47.78kHz to 0.61kHz, lower but somewhat similar to the range estimated from the Rosowski method. Because a small portion of the cochlea was unpreserved in our *Carsioptychus* specimen, these results represent minimum values, but should be close to the accurate figures. The values for *Carsioptychus* are compared to those of other extinct and extant mammals in Tables 6 and 7. Comparisons can also be made with hearing ranges for other living and fossil mammals in Figure 5 in Meng and Fox (1995).

In general, *Carsioptychus* had something of a 'standard' hearing range compared to other contemporaneous (or nearly contemporaneous) early placental mammals, and its values are most similar to those of *Alcidedorbignya* and *Hyopsodus*, particularly with the Rosowski (1992) equations. *Protungulatum* and *Diacodexis* had ranges that verged more slightly into the high-frequency spectrum. Notably, almost all of these extinct species fit within conventional hearing ranges of extant mammals. However, it may be argued that the extinct species have slightly higher-frequency sensitivities, but less of an ability to hear lower-frequency sounds, than extant mammals of similar body size. This observation requires

further testing with a broader sample of early mammal specimens, and perhaps a wider range of methods for predicting auditory ranges, like the equations Coleman and Boyer (2012) used to study primates.

Locomotor Agility

The equations based on semicircular canal radius (Silcox et al., 2009) provide an agility score between 2.49 and 2.99 for *Carsioptychus*. This indicates that *Carsioptychus* was a fairly slow moving animal with limited agility, broadly similar to modern pigs (*Sus scrofa*: 2.43-2.63). *Carsioptychus* has the lowest range of agility scores of any of the extinct Paleogene mammals in our comparative dataset (Table 8). Thus, even for its time, it was apparently a slow-moving mammal, although it should be noted that it was larger than the other Paleogene mammals in our dataset. The extinct species closest in agility to *Carsioptychus* is the pantodont *Alcidedorbignya* (score of 2.83-3.13), which also had below average agility. Other 'archaic' Paleogene mammals, like *Hyopsodus* and *Protungulatum*, had higher agility scores, roughly similar to modern gazelles but below the scores of particularly quick and agile small extant mammals like rabbits and squirrels (e.g., Spoor et al., 2007; Silcox et al., 2009a).

DISCUSSION

The CT data for *Carsioptychus coarctatus* (AMNH 27601) provide important new information on the brain, inner ears, and cranial vascularization of early placental mammals. This, in turn, provides insight into the origin of modern mammalian morphologies and helps reveal how the earliest Paleogene mammals were sensing their world during their initial radiation and the recovery from the end-Cretaceous extinction.

Evolution of the Placental Brain and Inner Ear

The overall morphology of the endocast of *Carsioptychus* suggests the brain was relatively primitive, with few modifications to the inferred ancestral eutherian/placental condition. Salient 'primitive' features include the large and anteriorly exposed olfactory bulbs, the conjoined olfactory bulbs (state 0 for character 4481 in O'Leary et al., 2013), the proportionally small neocortex, the lissencephalic cerebrum, and a large hindbrain compared to the cerebrum (e.g., Rowe et al., 2011). When features of the inner ear are scored for the phylogenetic characters of Macrini et al. (2013), *Carsioptychus* possesses the inferred primitive state of Placentalia for all characters that can be assessed, with only one exception: the lsc is the roundest canal in the placental ancestor, whereas the asc is the roundest canal in *Carsioptychus* (character 7) (see character scores in Table 9). Among these features, one of the most striking 'primitive' attributes of *Carsioptychus* is the presence of a secondary common crus, which is lost in more derived placentals (see also Orliac and O'Leary, 2016).

Perhaps the most notable 'primitive' feature of the *Carsioptychus* brain is its small overall size in relation to the surrounding cranium, although this is a qualitative observation and cannot be confirmed quantitatively with an EQ score because of the crushed nature of the specimen (see above). Table 4 provides comparative EQ measurements for a range of other early placental mammals. Some of these mammals, notably *Arctocyon*, *Meniscotherium*, *Phenacodus*, and *Pleuraspidotherium*, have EQs near the threshold value of 0.25 that was recently considered a hallmark feature of the placental ancestor by O'Leary et al. (2013). Furthermore, two Paleogene taxa have much lower EQs, within the non-mammalian cynodont range: *Barylambda* (0.10-0.11: Silcox et al, 2010) and *Onychodectes* (0.08-0.10: Napoli et al., 2017). We hypothesize that *Carsioptychus* also had an EQ value somewhere

around the 0.25 threshold; this can hopefully be tested with the discovery of more complete fossils in the future. However, it is worth noting that the evolution of EQ in placental mammals appears to be more complex than a simple 'placental cutoff' implies. Many non-crown group mammals have EQ values above the 0.25 threshold (e.g., Rowe et al., 2011; O'Leary et al., 2013), and in fact, Rowe et al. (2011) considered 0.50 to be the hallmark of the modern 'mammalian range' (see also Hoffmann et al., 2014).

Therefore, many Paleogene mammals (including potentially *Carsioptychus*) had lower EQ values than most modern placentals, and perhaps even substantially lower than the placental common ancestor and deeper nodes in cynodont phylogeny. The interpretation of this pattern awaits further testing, with a broader dataset of EQ values in extinct mammals and phylogenetic comparative methods. This will help untangle whether this observation represents a statistically robust pattern, and if so, whether it reflects the preferential survival of small-brained species across the Cretaceous-Paleogene boundary, a reversal to smaller brains after the extinction in the Paleogene, or an allometric constraint imposed by the initial evolution of larger body size in Paleogene placentals after the dinosaurs died. Whatever the explanation, however, it appears as if many Paleogene placental mammals had generally low intelligence compared to modern placentals, and perhaps many of their ancestors.

Senses and Behaviors of Paleogene Mammals

The posterior portion of the cranium of *Carsioptychus* is transversely expanded relative to the height of the braincase, which is also the case in other closely related periptychids, such as *Periptychus* and *Ectoconus* (Matthew, 1937). Several bones in this region are enlarged, notably the squamosal, parietal, and mastoid. This would have allowed for a greater surface area for muscle attachment, particularly for the temporalis muscle that elevates and retracts the mandible during feeding (Herring, 2007; Evans and De Lahunta, 2012), which may have

served to increase the power and efficiency of the jaws of *Carsioptychus*. There are features of the vascular system, observable in the CT data, which correspond to this large muscle mass. Twelve foramina are present on the parietal and squamosal external surfaces. These would have likely increased blood supply and drainage to the temporal region. Additionally, the enlargement of the bones in this region is counteracted by enlarged lateral sinuses, which would have served to lighten the skull. A similar condition has been observed in some other mammals, and has been interpreted to provide a larger surface area for masticatory muscles without greatly increasing skull mass (Murray, 1992; Sharp, 2016).

Our calculations, based on the dimensions of the cochlea and semicircular canals, suggest that *Carsioptychus* had generally 'conventional' hearing for a placental mammal, but was not particularly agile. Other Paleogene mammals had similar hearing ranges (Tables 6-7), suggesting that, to a first approximation, the standard hearing baseline of modern placentals was already established by this point in their history. Not all Paleogene mammals, however, had agility scores as low as *Carsioptychus*, and some are predicted to have been as agile as extant gazelles (Table 8). This indicates that placentals had developed a range of lifestyles, corresponding to different agility scores, by the Paleogene, which is not particularly surprising given the great diversity of habitat and lifestyle in their Mesozoic ancestors (Luo, 2007).

Putting this information together, it seems as if *Carsioptychus* used its strong jaw muscles, in combination with its thick bunodont teeth (Rose, 2006), to consume coarse and/or hard foods, such as nuts or rough foliage. It is also possible that *Carsioptychus* was able to locate foods beneath the ground such as tubers, using its acute sense of smell enabled by its large olfactory bulbs. Its agility was roughly similar to that of modern pigs, although its body proportions would have been much different (e.g., Shelley et al., in review). It was but one of

many different types of mammals exploiting new diets, behaviors, and lifestyles in the aftermath of the dinosaur extinction.

ACKNOWLEDGEMENTS

This project stemmed from JC's the MEarthSci dissertation at the University of Edinburgh, supervised by SLB, SS, and TEW. We thank Hong-yu Yi for CT scanning the specimen at AMNH, and Meng Jin for providing permission to scan the specimen under his care. We thank Mary Silcox and two anonymous reviewers for their comments, which greatly improved the manuscript. SLS was supported by a Natural Environment Research Council PhD studentship. TEW and SLB were supported by a National Science Foundation grant (EAR 1325544) and the Bureau of Land Management. SLB was supported by funding from the European Research Council (ERC) under the European Union's Horizon 2020 research and innovation programme (grant agreement No 756226, ERC Starting Grant: PalM), a Marie Curie Career Integration Grant (EC 630652), Royal Society Research Grant (RG130018), and the University of Edinburgh School of GeoSciences.

LITERATURE CITED

Alroy J. 1999 The fossil record of North American mammals: evidence for a Paleocene evolutionary radiation. Syst. Biol. 48:107–118.

Archibald JD, Clemens WA, Gingerich PD, Krause DW, Lindsay EH, Rose KD. 1987. First North American Land Mammal Ages of the Cenozoic Era. In: Woodburne MO, editor. Cenozoic Mammals of North America. Berkeley: University of California Press, p. 24-76.

Archibald JD 1998. Archaic ungulates ("Condylarthra"). In: Janis CM, Scott KM, Jacobs LJ, editors. Evolution of Tertiary Mammals of North America: Volume 1, Terrestrial Carnivores, Ungulates. Cambridge: Cambridge University Press, p. 292-329.

Archibald JD, Deutschman DH. 2001. Quantitative analysis of the timing of origin of extant placental orders. J Mamm Evol 8:107–124.

Averianov, A., Martin, T., Lopatin, A. 2013. A new phylogeny for basal Trechnotheria and Cladotheria and affinities of South American endemic Late Cretaceous mammals: Naturwissenschaften 100:311-326.

Bertrand OC, Amador-Mughal F, Silcox MT. 2016. Virtual endocasts of Eocene *Paramys* (Paramyinae): oldest endocranial record for Rodentia and early brain evolution in Euarchontoglires. Proc R Soc B 283:20152316.

Billet G, Muizon C, Schellhorn R, Ruf I, Ladevèze S, Bergqvist L. 2015. Petrosal and inner ear anatomy and allometry amongst specimens referred to Litopterna (Placentalia). Zool J Linn Soc 173:956-987.

Black D. 1920. Studies on endocranial anatomy. II. On the endocranial anatomy of *Oreodon* (Merycoidodon). J Comp Neuro 32:271–327.

Butler AB, Hodos W. 1996. Comparative vertebrate anatomy. London: Wiley-Liss.

Campione NE, Evans DC. 2012. A universal scaling relationship between body mass and proximal limb bone dimensions in quadrupedal terrestrial tetrapods. BMC Biol 10(1):60.

Coleman MN, Boyer DM. 2012. Inner ear evolution in primates through the Cenozoic: implications for the evolution of hearing. Anat Rec 295:615-631.

Cope ED. 1880. On the foramina perforating the posterior part of the squamosal bone of the Mammalia. Proc Am Phil Soc 18:452-461.

Cope ED. 1883. On some fossils of the Puerco Formation: Acad Nat Sci Phil Trans, 1883.

dos Reis M, Donoghue PCJ, Yang Z 2014. Neither phylogenomic nor palaeontological data support a Palaeogene origin of placental mammals. Biol Lett 10:20131003.

dos Reis M, et al. 2012. Phylogenomic datasets provide both precision and accuracy in estimating the timescale of placental mammal phylogeny. Proc Biol Sci 279: 3491–3500.

Døving KB, Trotier D. 1998. Structure and function of the vomeronasal organ. J Exp Biol 201:2913-2925

Eisenberg JF, Wilson DE. 1981. Relative brain size and demographic strategies in didelphid marsupials. Am Nat 118:1-15.

Ekdale EG. 2013. Comparative anatomy of the bony labyrinth (inner ear) of placental mammals. PLoS One 8(6):e66624.

Ekdale EG. 2016. Form and function of the mammalian inner ear. J Anat 228:324-337.

Evans HE, De Lahunta A. 2012. Miller's Anatomy of the Dog. Amsterdam: Elsevier Health Sciences.

Gelfo, J. N., Goin, F. J., Woodburne, M. O., Muizon, C. d. 2009. Biochronological relationships of the earliest South American Paleogene mammalian faunas: Palaeontology 52:251-269.

Goswami A. 2012. A dating success story: genomes and fossils converge on placental mammal origins. EvoDevo 3:18.

Grossnickle D, Newham E. 2016. Therian mammals experience an ecomorphological radiation during the Late Cretaceous and selective extinction at the K-Pg boundary. Proc R Soc B 283:20160256.

Halliday TJD, Goswami A. 2016a. Eutherian morphological disparity across the end-Cretaceous mass extinction. Biol. J. Linn. Soc. Lond. 118:152–168.

Halliday TJD, Goswami A. 2016b. The impact of phylogenetic dating method on interpreting

trait evolution: a case study of Cretaceous–Palaeogene eutherian body-size evolution. Biol Lett 12:20160051.

Halliday TJD, Upchurch P, Goswami A. 2016. Eutherians experienced elevated evolutionary rates in the immediate aftermath of the Cretaceous–Palaeogene mass extinction. Proc R Soc B 283:20153026.

Herring SW. 2007. Masticatory muscles and the skull: a comparative perspective. Arch Oral Biol 52:296-299.

Hoffmann, S. et al. 2014. Endocranial and inner ear morphology of *Vintana sertichi* (Mammalia, Gondwanatheria) from the Late Cretaceous of Madagascar. J. Vert. Paleontol. 34(sup1):110–137.

Jerison HJ. 1973. Evolution of the Brain and Intelligence. New York: Academic Press.

Keverne EB. 1999. The vomeronasal organ. Science 286:716-720.

Kielan-Jaworowska Z. 1986. Brain Evolution of Mesozoic Mammals. Rocky Mtn Geol 24 (special paper 3):21-34.

Legendre S. 1989. Les communautés de mammiéres du Paléogène (Eocène supérieur et Oligocène) d'Europe occidentale: structures, milieux et évolution. Münchner Geowissenschaftliche Abhandlungen, Reihe A, Geologie und Paläontologie 16:1-110.

Liem K, Bemis, W, Walker WF, Grande L. 2001. Functional anatomy of the vertebrates: an evolutionary perspective. W.H. Freeman.

Liu L et al. 2017. Genomic evidence reveals a radiation of placental mammals uninterrupted by the KPg boundary. Proc Nat Acad Sci USA 114:E7282-E7290.

Lofgren DL, Lillegraven JA, Clemens WA, Gingerich PD, Williamson TE, Woodburne MO. 2004. Paleocene biochronology: the Puercan through Clarkforkian land mammal ages. In Woodburne MO, editor. Late Cretaceous and Cenozoic Mammals of North

America. Biostratigraphy Geochronology, Columbia University Press New York. 2004 p. 43–105.

Luo Z-X. 2007. Transformation and diversification in early mammal evolution. Nature 450:1011-1019.

MacPhee RDE. 1994. Morphology, adaptations, and relationships of *Plesiorycteropus*: and a diagnosis of a new order of eutherian mammals. Bull Am Mus Nat Hist 220:1-214.

Macrini TE, De Muizon C, Cifelli RL, Rowe T. 2007. Digital cranial endocast of *Pucadelphys andinus*, a Paleocene metatherian. J Vert Paleontol, 27:99-107.

Macrini TE, Flynn JJ, Ni X, Croft DA, Wyss AR. 2013. Comparative study of notoungulate (Placentalia, Mammalia) bony labyrinths and new phylogenetically informative inner ear characters. J Anat 223:442-461.

Malinzak MD, Kay RF, Hullar TE. 2012. Locomotor head movements and semicircular canal morphology in primates. Proc Nat Acad Sci USA, 109:17914-17919.

Maor R, Dayan T, Ferguson-Gow H, Jones KE. 2017. Temporal niche expansion in mammals from a nocturnal ancestor after dinosaur extinction. Nat Ecol Evol 1:1889-1895.

Martínez G, Dozo MT, Gelfo JN, Marani H. 2016. Cranial Morphology of the Late Oligocene Patagonian notohippid *Rhynchippus equinus* Ameghino, 1897 (Mammalia, Notoungulata) with Emphases in Basicranial and Auditory Region. PLoS ONE 11(5):e0156558.

Matthew WD. 1937. Paleocene faunas of the San Juan Basin, New Mexico. In Granger W, Gregory WK, Colbert EH, editors. Transactions of the American Philosophical Society, new series, vol. XXX p. 1-510.

McDowell SB. 1958. The Greater Antillean insectivores. Bull Am Mus Nat Hist 115(3): 113-214.

Meng J, Fox RC. 1995. Osseous inner ear structures and hearing in early marsupials and

placentals. Zool J Linn Soc 115:47-71.

Meredith RW et al. 2011. Impacts of the Cretaceous Terrestrial Revolution and KPg extinction on mammal diversification. Science 334:521–524.

Muizon CD, Billet G, Argot C, Ladevèze S, Goussard F. 2015. *Alcidedorbignya inopinata*, a basal pantodont (Placentalia, Mammalia) from the early Palaeocene of Bolivia: anatomy, phylogeny and palaeobiology. Geodiversitas 37:397-634.

Murphy WJ et al. 2001 Molecular phylogenetics and the origins of placental mammals. Nature 409:614–618.

Muller M. 1994. Semicircular duct dimensions and sensitivity of the vertebrate vestibular system. J Theor Biol 167:239-256.

Murray PF. 1992. Thinheads, thickheads and airheads - Functional craniology of some diprotodontian marsupials. Beagle: Records of the Museums and Art Galleries of the Northern Territory 9:71-87.

Napoli JG, Williamson TE, Shelley SL, Brusatte SL. 2017. A digital endocranial cast of the early Paleocene (Puercan) 'archaic' mammal *Onychodectes tisonensis* (Eutheria: Taeniodonta). J Mammal Evol DOI 10.1007/s10914-017-9381-1.

Nieuwenhuys R, Donkelaar HJ, Nicholson C. 1998. The Central Nervous System of Vertebrates. Berlin: Springer.

O'Leary MA et al. 2013. The placental mammal ancestor and the post–K-Pg radiation of placentals. Science 339:662-667.

Oman CM, Marcus EN, Curthoys IS. 1987. The influence of the semicircular canal morphology on endolymph flow dynamics. Acta Otolaryngol 103:1-13.

Orliac MJ, Argot C, Gilissen E. 2012a. Digital cranial endocast of *Hyopsodus* (Mammalia, "Condylarthra"): a case of Paleogene terrestrial echolocation? PLoS ONE, 7(2):e30000.

Orliac MJ, Benoit J, O'Leary MA. 2012b. The inner ear of *Diacodexis*, the oldest artiodactyl mammal. J Anat 221:417-426.

Orliac MJ, Gilissen E. 2012. Virtual endocranial cast of earliest Eocene *Diacodexis* (Artiodactyla, Mammalia) and morphological diversity of early artiodactyl brains. Proc R Soc Lond B 279:3670-3677.

Orliac MJ, O'Leary MA. 2016. The inner ear of *Protungulatum* (Pan-Euungulata, Mammalia). J Mammal Evol 23:337-352.

Prothero DR, Manning EM, Fischer M. 1988. The phylogeny of the ungulates. In: Benton MJ, editor. The Phylogeny and Classification of the Tetrapods 2. Clarendon Press Oxford, p. 201–234.

Ravel A, Orliac M.J. 2015. The inner ear morphology of the 'condylarthran' *Hyopsodus lepidus*. Hist Biol 27:957-969.

Rose KD. 2006. The beginning of the age of mammals. Baltimore: Johns Hopkins University Press.

Rosowski JJ. 1992. Hearing in transitional mammals: tredictions from the middle-ear anatomy and hearing capabilities of extant mammals. In: Webster DB, Popper AN, Fay RR, editors. The Evolutionary Biology of Hearing. New York: Springer, p. 615-631.

Rowe TB. 1996. Coevolution of the mammalian middle ear and neocortex. Science 273:651-654.

Rowe TB, Macrini TE, Luo Z-X. 2011. Fossil evidence on origin of the mammalian brain. Science 332:955-957.

Schwarz DWF, Tomlinson RD. 1994. Physiology of the vestibular system. In: Jackler RK, Brackmann DE editors. Neurotology. St.Louis: Mosby, pp. 59–98.

Sharp AC. 2016. A quantitative comparative analysis of the size of the frontoparietal sinuses

and brain in vombatiform marsupials. Mem Mus Vic 74:331-342.

Shelley SL. 2017. The rise of placental mammals: the anatomy, palaeobiology and phylogeny of *Periptychus* and the Periptychidae. Unpublished PhD Thesis, University of Edinburgh.

Shelley SL, Williamson TE, Brusatte SL. In review. The anatomy and palaeobiology of the Palaeocene mammal *Periptychus carinidens* (Periptychidae, Mammalia). PLoS ONE.

Silcox MT, Bloch JI, Boyer DM, Godinot M, Ryan TM, Spoor F, Walker A. 2009a. Semicircular canal system in early primates. J Human Evol 56:315-327.

Silcox MT, Dalmyn CK, Bloch JI. 2009b. Virtual endocast of *Ignacius graybullianus* (Paromomyidae, Primates) and brain evolution in early primates. Proc Nat Acad Sci USA 106:10987-10992.

Simpson GG. 1933. Braincasts of *Phenacodus*, *Notostylops*, and *Rhyphodon*. Am Mus Novitates 622:1-19.

Simpson GG. 1936a. Additions to the Puerco fauna, lower Paleocene. Am Mus Novitates 849:1–12.

Simpson GG. 1936b. *Carsioptychus*, new name for *Plagioptychus* Matthew. Am J Sci 32:234.

Slater GJ. 2013. Phylogenetic evidence for a shift in the mode of mammalian body size evolution at the Cretaceous-Paleogene boundary. Methods Ecol. Evol 4:734–744.

Spoor F, Bajpai S, Hussain ST, Kumar K, Thewissen JGM. 2002. Vestibular evidence for the evolution of aquatic behaviour in early cetaceans. Nature 417:163-166.

Spoor F, Garland T, Krovitz G, Ryan TM, Silcox MT, Walker A. 2007. The primate semicircular canal system and locomotion. Proc Nat Acad Sci USA 104:10808-10812.

Spoor F, Zonneveld F. 1998. Comparative review of the human bony labyrinth. Yb Phys Anthropol 41:211-251.

Taniguchi K., Saito S, Taniguchi K. 2011. Phylogenic outline of the olfactory system in vertebrates. J Vet Med Sci 73:139-147.

Van Valen L. 1978. The beginning of the age of mammals. Evol Theor 4:5–80.

West CD. 1985. The relationship of the spiral turns of the cochlea and the length of the basilar membrane to the range of audible frequencies in ground dwelling mammals. J Acou Soc Am 77:1091-1101.

Wible JR. 2008. On the cranial osteology of the Hispaniolan solenodon, *Solenodon paradoxus* Brandt, 1833 (Mammalia, Lipotyphla, Solenodontidae). Ann Carnegie Mus 77:321-402.

Wible JR, Hopson JA. 1993. Basicranial evidence for early mammal phylogeny. In Szalay FS, Novacek MJ, McKenna MC, editors. Mammal Phylogeny, Springer, New York, p. 45-62.

Wible JR, Novacek MJ, Rougier GW. 2004. New data on the skull and dentition in the Mongolian Late Cretaceous eutherian mammal *Zalambdalestes*. Bull Am Mus Nat Hist 281:1-144.

Wible JR, Rougier GW, Novacek MJ, Asher RJ. 2007. Cretaceous eutherians and Laurasian origin for placental mammals near the K/T boundary. Nature 447:1003-1006.

Wible JR, Rougier GW, Novacek MJ, Asher RJ. 2009. The eutherian mammal *Maelestes gobiensis* from the Late Cretaceous of Mongolia and the phylogeny of Cretaceous Eutheria. Bull Am Mus Nat Hist 327:1-123.

Williamson TE. 1996. The beginning of the age of mammals in the San Juan Basin, New Mexico; biostratigraphy and evolution of Paleocene mammals of the Nacimiento Formation. New Mexico Mus Nat Hist Sci Bull 8:1–141.

Wilson GP. 2013. Mammals across the K/Pg boundary in northeastern Montana, U.S.A.:

dental morphology and body-size patterns reveal extinction selectivity and immigrant-fueled ecospace filling. Paleobiology 39:429-469.

Wu J, Yonezawa T, Kishino H. 2017. Rates of molecular evolution suggest natural history of life history traits and a post-K-Pg nocturnal bottleneck of placentals. Curr Biol 27:1-9.

FIGURE CAPTIONS

Fig. 1. The cranium of the periptychid 'condylarth' mammal *Carsioptychus coarctatus* (AMNH 27601) in dorsal (A), ventral (B), right lateral (C) and left lateral (D) views. Abbreviations: al, alisphenoid; ar, auditory region (promontorium of petrosal); bo, basioccipital; bs, basisphenoid; ch, choanae; eam, external acoustic meatus; ?fo, foramen ovale; ma, mastoid; mp, mastoid protuberance; oc, occipital condyle; oev, foramen for exit of occipital emissary vein; pa, parietal; pgf, postglenoid foramen; pgp, postglenoid process; psc, parietal-squamosal contact; pt, pterygoid; sgf, supraglenoid foramen; sq, squamosal. Scale bar equals 5 cm.

Fig 2. Digital CT model of the endocast of the brain, inner ear, and cranial vessels of *Carsioptychus coarctatus*, within a transparent rendering of AMNH 27601, in dorsal (A), ventral (B), posterior (C), right lateral (D), and left lateral (E) views. Scale bar equals 5 cm.

Fig 3. Digital CT model and line drawings of the endocast of the brain, inner ear, and cranial vessels of *Carsioptychus coarctatus* (AMNH 27601) in right lateral (A-B), dorsal (C-D), and ventral (E-F) views. Abbreviations: aa, auditory apparatus; cbh, cerebral hemisphere; cev, capsuloparietal emissary vein; cf, circular fissure; coc, condyloid canal; dos, dorsum sellae; for, cast of canal for CN V2; hyp, hypophyseal cast; los, longitudinal sulcus; mdb, cast of canal for CN V3; mxb, cast of canal for CN V_2; nc, neocortex; ob, olfactory bulb; oev, occipital emissary vein; opb, cast of canal for CN III, IV, V_1, VI; otc, groove for the ossified tentorium cerebelli; pf, paraflocculus; pil, piriform lobe; ptc, posttemporal canal; rhf, rhinal

fissure; sdtm, sinus drain for the temporomandibular muscles; sis, sigmoid sinus; trs, transverse sulcus; ve, vermis; vnn, vomeronasal nerve canal cast. Scale bar equals 2 cm.

Fig. 4. Digital CT slices though the skull of *Carsioptychus coarctatus* (AMNH 27601) in posterior view highlighting the ossified tentorium cerebelli (A-B); lateral view of the cranium highlighting the ossified tentorium cerebelli (C-E); and lateral view of the cranium highlighting the cast of the vomeronasal canal (F-H). Abbreviations: ec, endocast; oc, occipital condyle; otc, ossified tentorium cerebelli; sc, sagittal crest; vcc, vomeronasal canal cast. Scale bars equal 2 cm.

Fig. 5. Closeup of the digital CT model of the cranium of *Carsioptychus coarctatus* (AMNH 27601), showing the left petrosal in ventral view, with the inner ear endocast in blue. The left image shows those portions of the inner ear cavity that are exposed on the specimen, and the right image shows the inner ear in situ within the petrosal. Abbreviations: aa, anterior ampulla; co, cochlear canal; la, lateral ampulla; lsc, lateral semicircular canal; pa, posterior ampulla; psc, posterior semicircular canal; scc, secondary common crus; va, vestibular aqueduct. Scale bar equals 4 mm.

Fig. 6. Digital CT model and line drawings of the left inner ear (bony labyrinth) endocast of *Carsioptychus coarctatus* (AMNH 27601) in medial (A-B), anterior (C-D), lateral (E-F), dorsal (G-H), anterolateral (I-J), ventral (K-L), and posterior (M-N) views. Thick lines at angles indicate directions of orientation (anterior, posterior, dorsal, ventral, lateral, medial). Abbreviations: aa, anterior ampulla; asc, anterior semicircular canal; cc, common crus; co, cochlear canal; la, lateral ampulla; lsc, lateral semicircular canal; pa, posterior ampulla; pbl,

primary bony lamina; psc, posterior semicircular canal; sbl, secondary bony lamina; scc, secondary common crus; va, vestibular aqueduct. Scale bar equals 2.5 mm.

Fig. 7. Digital CT models of *Carsioptychus coarctatus* (AMNH 27601) (A-D), *Protungulatum* sp. (Orliac and O'Leary, 2016) (E-H), and *Hyopsodus lepidus* (Ravel and Orliac, 2015) (I-L), in medial (A,E,I), anterior (B,F.J), lateral (C,G,D), and dorsal (D,H,L) views. Abbreviations: Abbreviations: acf, external aperture of the cochlear fossula; ca, cochlear aqueduct; cc, common crus; er, elliptical recess; fv, fenestra vestibuli; pbl, primary bony lamina; sbl, secondary bony lamina; scc, secondary common crus; sr, spherical recess; va, vestibular aqueduct. Scale bars equal 1 mm.

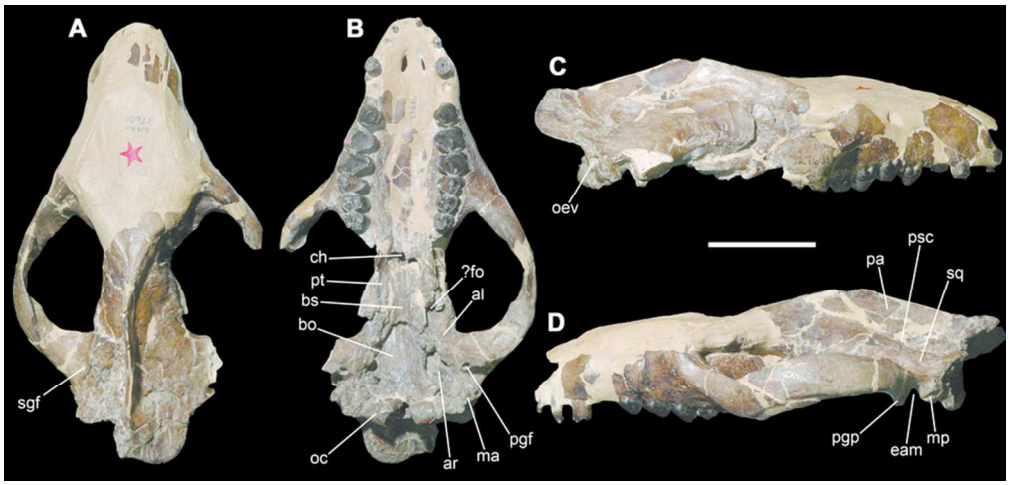

Fig. 1. The cranium of the periptychid 'condylarth' mammal Carsioptychus coarctatus (AMNH 27601) in dorsal (A), ventral (B), right lateral (C) and left lateral (D) views. Abbreviations: al, alisphenoid; ar, auditory region (promontorium of petrosal); bo, basioccipital; bs, basisphenoid; ch, choanae; eam, external acoustic meatus; ?fo, foramen ovale; ma, mastoid; mp, mastoid protuberance; oc, occipital condyle; oev, foramen for exit of occipital emissary vein; pa, parietal; pgf, postglenoid foramen; pgp, postglenoid process; psc, parietal-squamosal contact; pt, pterygoid; sgf, supraglenoid foramen; sq, squamosal. Scale bar equals 5 cm.

80x38mm (300 x 300 DPI)

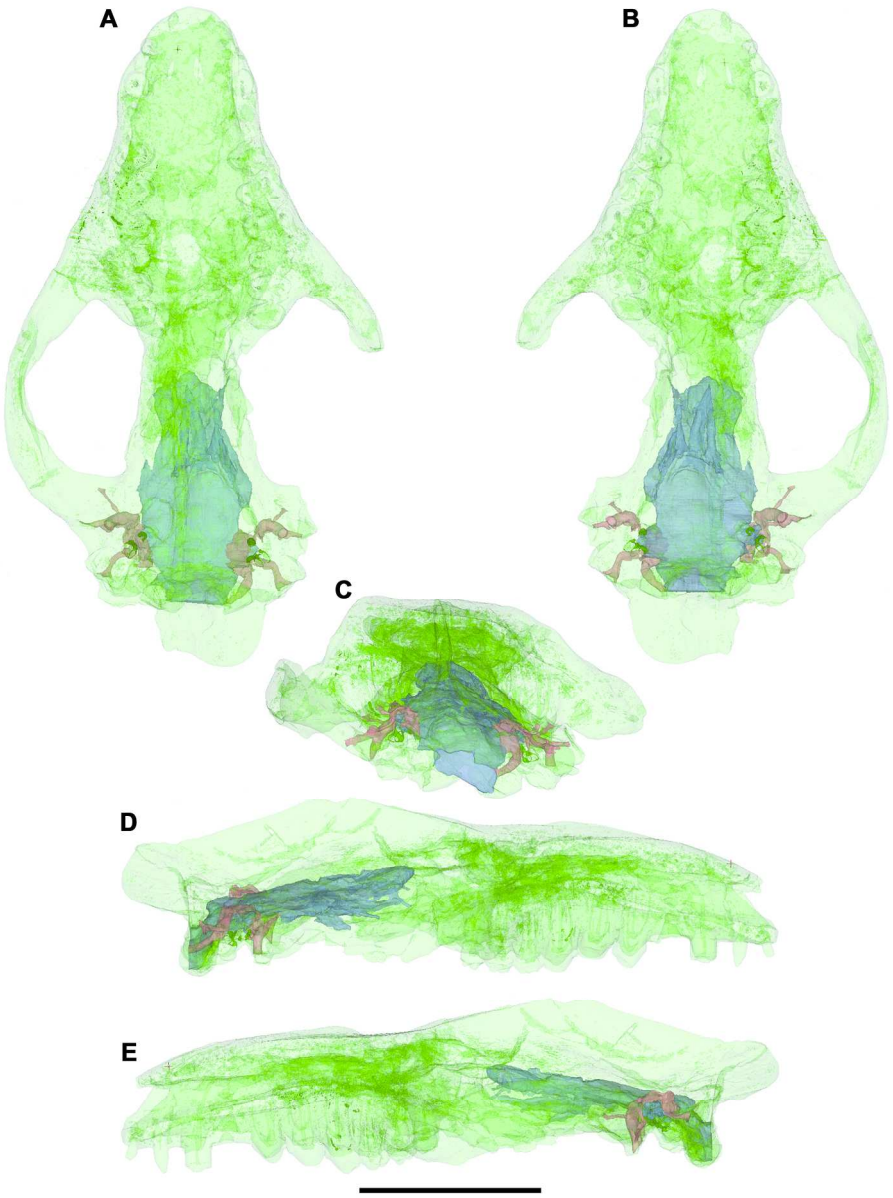

Fig 2. Digital CT model of the endocast of the brain, inner ear, and cranial vessels of Carsioptychus coarctatus, within a transparent rendering of AMNH 27601, in dorsal (A), ventral (B), posterior (C), right lateral (D), and left lateral (E) views. Scale bar equals 5 cm.

207x252mm (300 x 300 DPI)

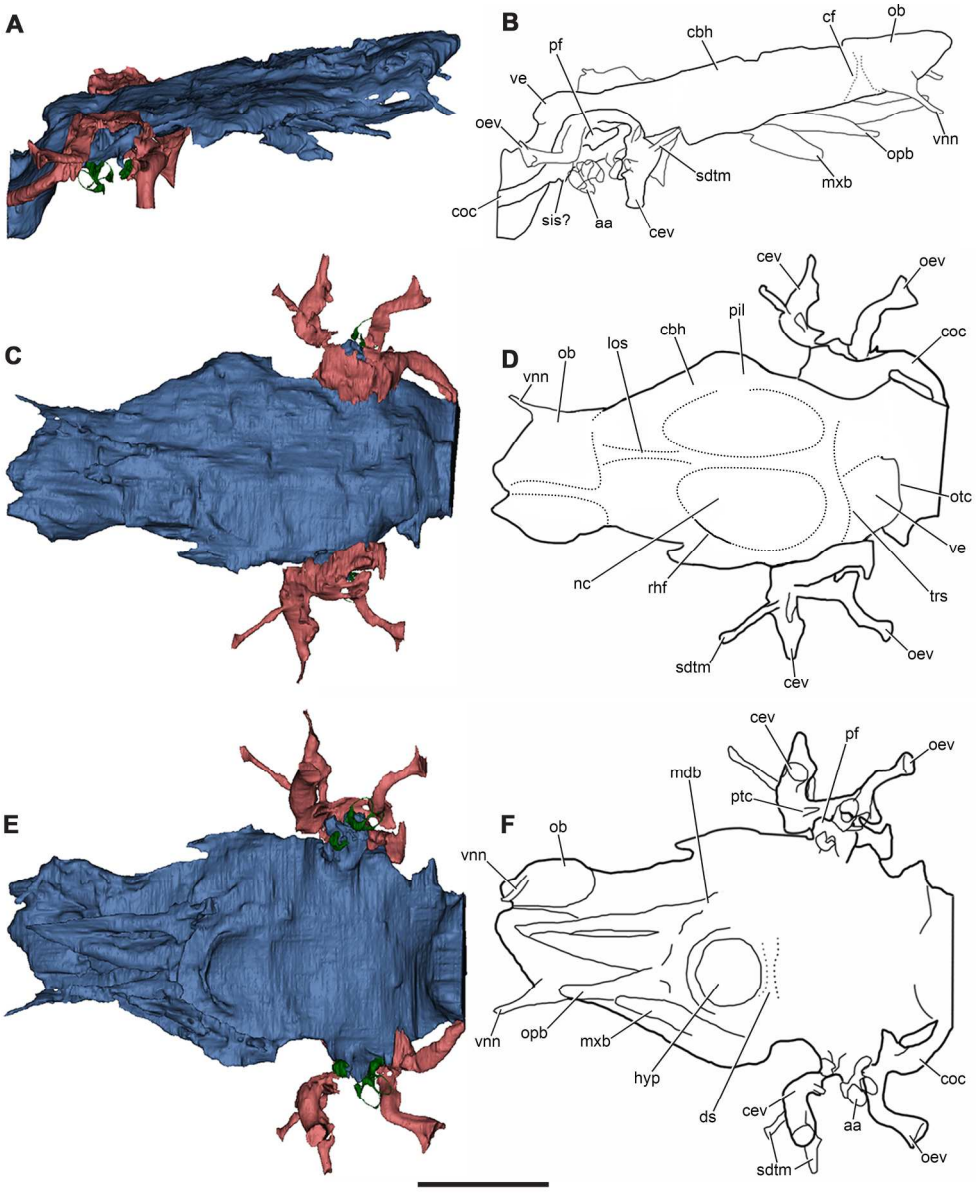

Fig 3. Digital CT model and line drawings of the endocast of the brain, inner ear, and cranial vessels of Carsioptychus coarctatus (AMNH 27601) in right lateral (A-B), dorsal (C-D), and ventral (E-F) views. Abbreviations: aa, auditory apparatus; cbh, cerebral hemisphere; cev, capsuloparietal emissary vein; cf, circular fissure; coc, condyloid canal; dos, dorsum sellae; for, cast of canal for CN V2; hyp, hypophyseal cast; los, longitudinal sulcus; mdb, cast of canal for CN V3; mxb, cast of canal for CN V2; nc, neocortex; ob, olfactory bulb; oev, occipital emissary vein; opb, cast of canal for CN III, IV, V1, VI; otc, groove for the ossified tentorium cerebelli; pf, paraflocculus; pil, piriform lobe; ptc, posttemporal canal; rhf, rhinal fissure; sdtm, sinus drain for the temporomandibular muscles; sis, sigmoid sinus; trs, transverse sulcus; ve, vermis; vnn, vomeronasal nerve canal cast. Scale bar equals 2 cm.

208x255mm (300 x 300 DPI)

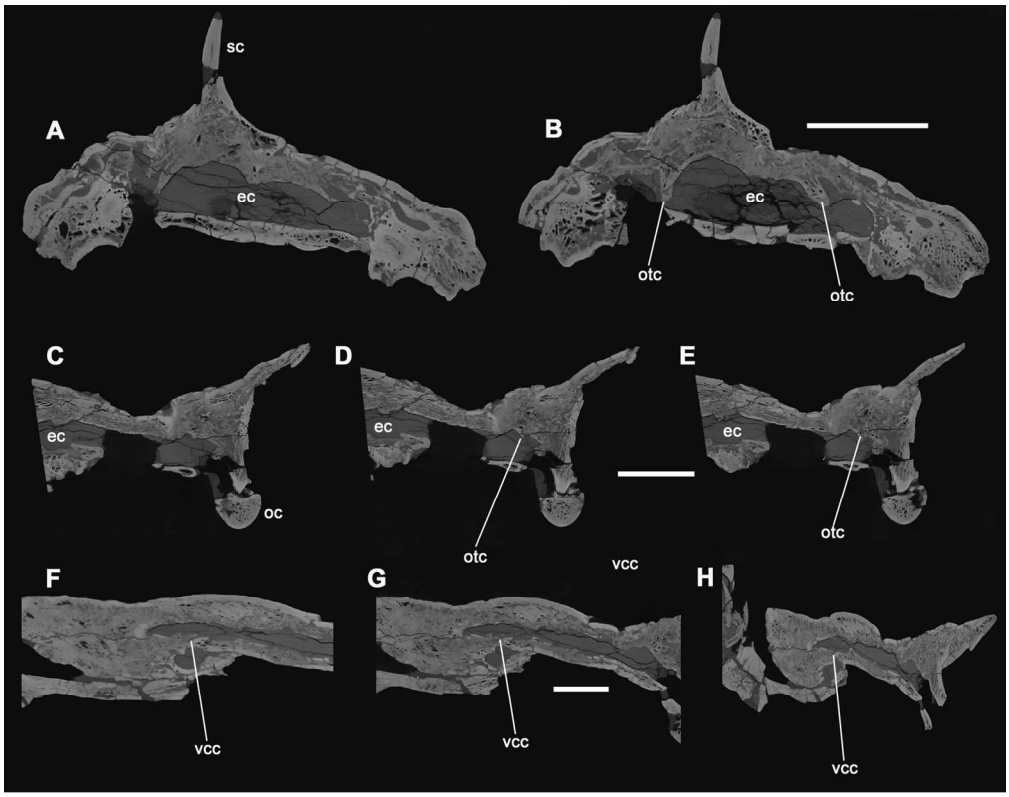

Fig. 4. Digital CT slices though the skull of Carsioptychus coarctatus (AMNH 27601) in posterior view highlighting the ossified tentorium cerebelli (A-B); lateral view of the cranium highlighting the ossified tentorium cerebelli (C-E); and lateral view of the cranium highlighting the cast of the vomeronasal canal (F-H). Abbreviations: ec, endocast; oc, occipital condyle; otc, ossified tentorium cerebelli; sc, sagittal crest; vcc, vomeronasal canal cast. Scale bars equal 2 cm.

133x104mm (300 x 300 DPI)

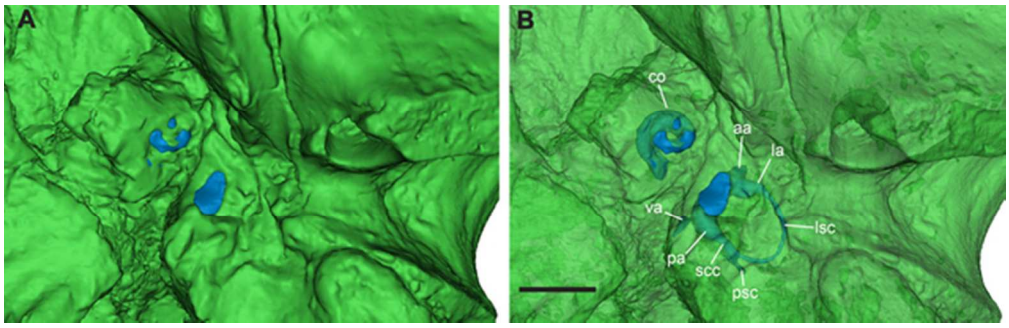

Fig. 5. Closeup of the digital CT model of the cranium of Carsioptychus coarctatus (AMNH 27601), showing the left petrosal in ventral view, with the inner ear endocast in blue. The left image shows those portions of the inner ear cavity that are exposed on the specimen, and the right image shows the inner ear in situ within the petrosal. Abbreviations: aa, anterior ampulla; co, cochlear canal; la, lateral ampulla; lsc, lateral semicircular canal; pa, posterior ampulla; psc, posterior semicircular canal; scc, secondary common crus; va, vestibular aqueduct. Scale bar equals 4 mm.

53x17mm (300 x 300 DPI)

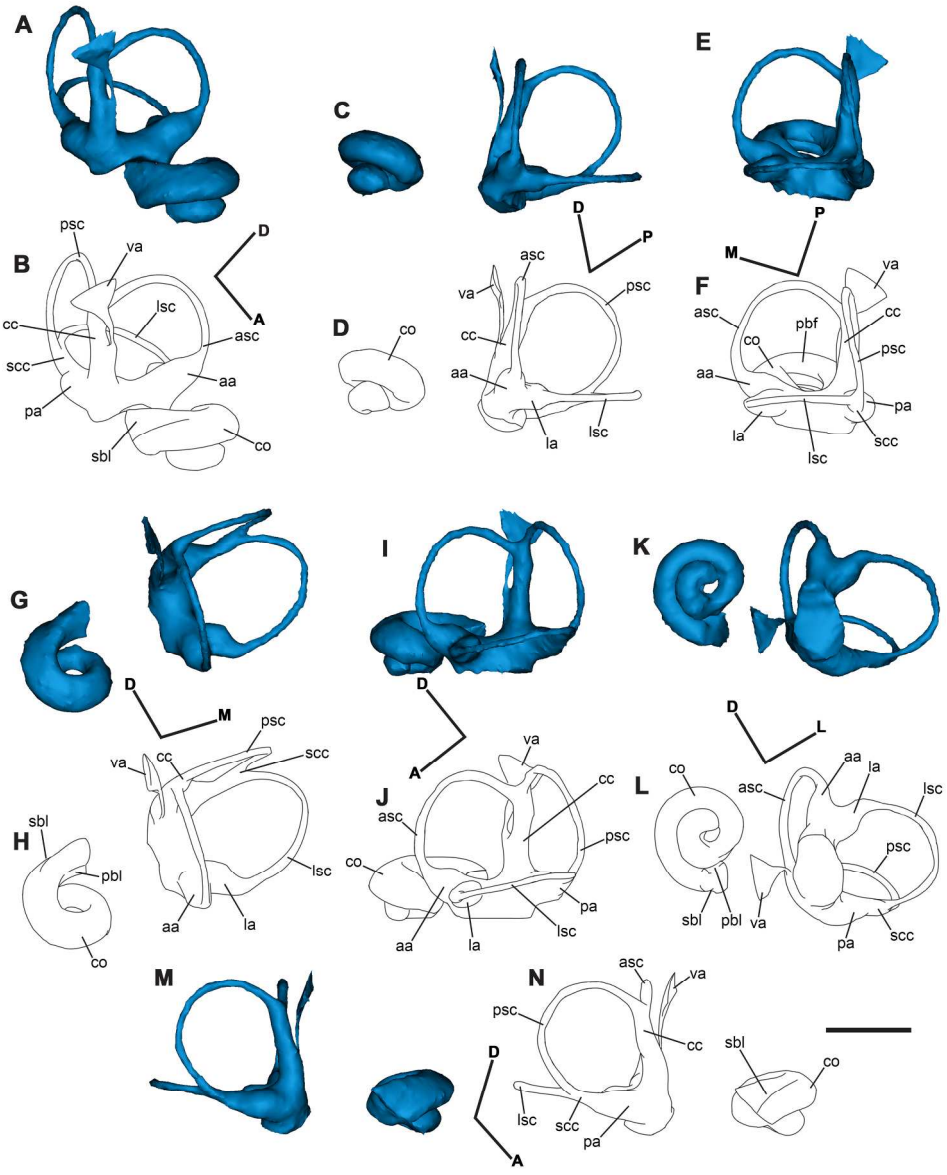

Fig. 6. Digital CT model and line drawings of the left inner ear (bony labyrinth) endocast of Carsioptychus coarctatus (AMNH 27601) in medial (A-B), anterior (C-D), lateral (E-F), dorsal (G-H), anterolateral (I-J), ventral (K-L), and posterior (M-N) views. Thick lines at angles indicate directions of orientation (anterior, posterior, dorsal, ventral, lateral, medial). Abbreviations: aa, anterior ampulla; asc, anterior semicircular canal; cc, common crus; co, cochlear canal; la, lateral ampulla; lsc, lateral semicircular canal; pa, posterior ampulla; pbl, primary bony lamina; psc, posterior semicircular canal; sbl, secondary bony lamina; scc, secondary common crus; va, vestibular aqueduct. Scale bar equals 2.5 mm.

213x269mm (300 x 300 DPI)

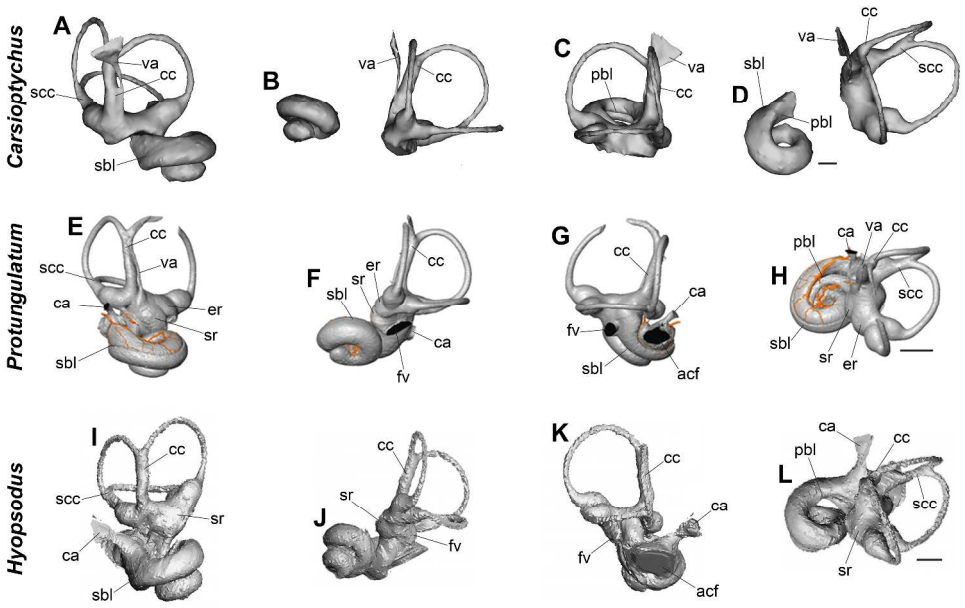

Fig. 7. Digital CT models of Carsioptychus coarctatus (AMNH 27601) (A-D), Protungulatum sp. (Orliac and O'Leary, 2016) (E-H), and Hyopsodus lepidus (Ravel and Orliac, 2015) (I-L), in medial (A,E,I), anterior (B,F.J), lateral (C,G,D), and dorsal (D,H,L) views. Abbreviations: Abbreviations: acf, external aperture of the cochlear fossula; ca, cochlear aqueduct; cc, common crus; er, elliptical recess; fv, fenestra vestibuli; pbl, primary bony lamina; sbl, secondary bony lamina; scc, secondary common crus; sr, spherical recess; va, vestibular aqueduct. Scale bars equal 1 mm.

TABLES

Agility Scores (for anterior, posterior, lateral and the average of semi-circular canals) (Silcox *et al*. 2009)	Anterior Canal Score: $\log_{10}(\text{Agility}) = 0.850 - 0.153\ (\log_{10}(\text{BM})) + (0.706\ (\log_{10}(\text{ASCR})))$ Posterior Canal Score: $\log_{10}(\text{Agility}) = 0.881 - 0.151\ (\log_{10}(\text{BM})) + (0.677\ (\log_{10}(\text{PSCR})))$ Lateral Canal Score: $\log_{10}(\text{Agility}) = 0.959 - 0.1670\ (\log_{10}(\text{BM})) + (0.854\ (\log_{10}(\text{LSCR})))$ Average Canal Score: $\log_{10}(\text{Agility}) = 0.948 - 0.188\ (\log_{10}(\text{BM})) + (0.962\ (\log_{10}(\text{SCR})))$	
Hearing Range at 60dB (Rosowski, 1992)	Low-Frequency Limit = $13(\text{BML})^{-1.2}$	High-Frequency Limit = $391(\text{BML})^{-0.85}$
Hearing Range at 60dB (West, 1985)	$\log_{10}(\text{Low-Frequency Limit}) = 1.76\text{-}1.66\log_{10}(\text{BML*N})$	$\log_{10}(\text{High-Frequency Limit}) = 2.42\text{-}0.994\log_{10}(\text{BML/N})$

Table 1. Equations used to calculate agility scores and hearing range. Abbreviations: BM = body mass (grams); ASCR = anterior semi-circular canal radius (mm); PSCR = posterior semi-circular canal radius (mm); LSCR = lateral semi-circular canal radius (mm); SCR = average semi-circular canal radius (mm); BML =cochlear basilar membrane length (mm); N = number of cochlear turns.

Specimen	M_1 length	M_1 width	M_1 area	Mass (g)
NMMNH P-56929	5.69	9.76	55.5344	8933.79287
AMNH 113998	8.55	6.97	59.5935	10699.4484
AMNH 839	9.18	8.76	80.4168	18498.7163
AMNH 3777	9.14	7.63	69.7382	14259.1633
UCM	8.67	7.36	63.8112	12123.267
				12902.88

Table 2. Lower molar tooth measurements and resultant body mass estimations for five specimens of *Carsioptychus coarctatus*, used to derive an average value to be used as a proxy for the body mass of AMNH 27601 in agility score equations (Table 1). Measurements of first lower molar m_1 are in mm/mm^2. The Legendre (1989) equation is: $\log_{10}(BM) = 1.827(\log_{10}(m_1 area))+1.810$. This equation was chosen because body mass estimates derived from it provide the closest match to body mass estimates derived from long bone circumference equations (established to be the most accurate way of estimating body mass in quadrupedal animals: Campione and Evans, 2012) in the closely related *Periptychus* (Shelley, 2017; Shelley et al., in review).

Endocast Maximum Length	69.45
Endocast Maximum Width	34.69
Olfactory Bulb Length	20.92
Olfactory Bulb Width (total of both bulbs)	21.05
Cerebrum Length	33.54
Cerebrum Width	34.69
Midbrain dorsal exposure length	4.79
Hindbrain Length	15.07
Hindbrain Width	25.43
Hypophyseal Cast Length	9.53
Hypophyseal Cast Width	10.84
Endocast Volume	7876

Table 3. Endocast measurements for *Carsioptychus coarctatus* (AMNH 27601). Linear measurements are given in mm; volume measurements are given in mm^3. The olfactory bulb and cerebrum width estimate values are double the value of the less deformed left side. The volume measurement is the observed value but is severely underestimated due to crushing.

Species	EV (cm3)	BM (g)	EQ (Eisenberg and Wilson, 1981)	EQ (Jerison, 1973)
Hyopsodus lepidus	2.79	633	0.43	0.31
Arctocyon primaevus	37	29700-40800	0.26-0.33	0.26-0.32
Arctocyonides areane	12	3900-5400	0.38-0.48	0.32-0.40
Phenacodus primaevus	35	52800	0.20	0.21
Meniscotherium meniscum	12	6800-9100	0.25-0.32	0.23-0.28
Pleuraspidotherium	6	3300	0.27	0.22
Mesonyx obrusidens	80	35400-47200	0.50-0.62	0.51-0.62
Hyracotherium sp.	25	9068	0.54	0.48
Homacodon vagans	9.5	720-1010	1.03-1.33	0.78-0.98
Alcidedorbignya inopinata	2.2	483	0.41	0.29

Table 4. The encephalization quotient (EQ) of early placental mammals ('condylarths', basal ungulates, and the pantodont *Alcidedorbignya*). The two versions of EQ are calculated using the protocols of Eisenberg and Wilson (1981) and Jerison (1973). Values for basal ungulate examples are from Orliac *et al.* (2012a), and *Alcidedorbignya* values are from Muizon *et al.* (2015). The EQ of *Carsioptychus* cannot be calculated at this time because of the deformation of the anterior and middle portions of the endocast. Abbreviations: BM, body mass; EQ, encephalization quotient; EV, endocranial volume.

Measurement	*C. coarctatus*	*Protungulatum*	*H. lepidus*	*D. ilicis*	*A. inopinata*	Zhelestids	*K. kulbecke*	*Z. lechei*
Cochlear Aspect Ratio	0.70	0.51	0.77	0.54	0.40-0.48	0.46	0.44	0.4
Cochlear Coiling	1.67 turns / 600°	1.54 turns / 553°	2.25 turns / 765°	2 turns / 720°	1.5 turns / 540°	1.5 turns / 518°	1.2 turns / 446°	1 turn / 368°
Cochlear Canal Length	9.27	7.10	10.10	7.35	8.48-10.86	Average of 4.93	4.93	3.4
Cochlear Volume	7.25	3.10	7.19	6.53	-	-	-	2.9
2° Lamina Coil	130°	340°	135°	180°	90°	198°	209°	95.3°
Basal Turn/LSC Angle	29°	-	20°	13°	21°-35°	34°	12.1°	13.5°
ASC/LSC	80°	74°	92°	73°	84°-87°	88.8°	79.9°	-
LSC/PSC	80°	98°	91°	81°	90°	93.1°	89.6°	-
ASC/PSC	90°	81°	84°	95°	69°-90°	96.8°	79.9°	-
ASC R	1.77	1.18	1.48	1.71	1.07-1.13	1.17	1.19	1.5
ASC L	7.90	5.97	7.20	8.69	7.21-7.42	5.80	5.70	6.9
ASC H	3.48	2.46	3.12	3.49	2.25-2.27	-	-	-
ASC W	3.61	2.27	2.81	3.36	2.00-2.26	-	-	-
PSC R	1.73	1.02	1.19	1.37	1.01	0.86	0.96	1.20
PSC L	9.58	5.79	7.1	7.68	6.51	4.62	4.55	5.9
PSC H	3.74	2.16	2.43	2.39	2.01	-	-	-
PSC W	3.19	1.94	2.36	3.09	2.03	-	-	-
LSC R	1.73	0.94	1.12	1.24	0.89-1.03	0.79	0.92	1.2
LSC L	7.33	4.23	5.43	5.05	5.81-6.80	3.49	3.94	5.20
LSC H	3.88	1.95	2.34	2.17	1.77-2.05	-	-	-
LSC W	3.02	1.82	2.14	2.79	1.79-2.06	-	-	-

Table 5. Measurements of the left inner ear bony labyrinth endocast of *Carsioptychus* and comparisons with other Paleocene-Eocene mammals (*Protungulatum* sp.: Orliac and O'Leary, 2016; *Hyopsodus lepidus*: Ravel and Orliac, 2015 and Orliac and O'Leary, 2016; *Diacodexis ilicis*: Orliac et al., 2012b; *Alcidedorbignya inopinata*: Muizon et al., 2015) and Mesozoic zhelestids (*Kulbeckia kulbecke* and *Zalambdalestes lechei*: Ekdale, 2013). Linear measurements are in mm, volume measurements are in mm^3. Value ranges for *Alcidedorbignya* are based on different petrosal specimens. Given the poor preservation at the base of the cochlear turn in *Carsioptychus*, cochlear measurements represent minimum values, although true values are unlikely to be substantially different because only a small portion was unpreserved.

Abbreviations: ASC, anterior semicircular canal; LSC, lateral semicircular canal; PSC, posterior semicircular canal; R, L, W, H = radius, length, width, and height.

Species	Low-Frequency Limit (kHz)	High-Frequency Limit (kHz)
Sus scrofa (Wild boar)	0.30	27.31
Homo sapiens (Human)	0.31	27.72
Litopterns (21.16mm)	0.33	29.20
Felis catus (Cat)	0.44	35.54
Litopterns (16.55mm)	0.45	35.99
Orycteropus afer (Aardvark)	0.51	39.35
Canis familiaris (Dog)	0.55	41.75
Alcidedorbignya	0.74	51.49
Hyopsodus	0.81	54.77
Carsioptychus	0.90	58.70
Sylvilagus floridanus (Rabbit)	0.96	61.87
Didelphis virginiana (Opossum)	1.15	70.21
Diacodexis	1.18	71.75
Protungulatum	1.21	73.91
Atelerix albiventris (Hedgehog)	1.15	99.72
Kulbeckia	1.92	100.75
Zhelestids	1.92	100.75
Mus musculus (Mouse)	2.56	123.77
Zalambdelestes	2.99	138.17

Table 6. Low and high-frequency limits of hearing at 60 dB in kHz (based on Rosowski's [1992]) equations) for a range of extant and extinct mammals. Two ranges for litopterns are shown, based on different petrosal specimens with different basilar membrane lengths (Billet et al., 2015). Data for extant and Mesozoic mammals are from Ekdale (2013). Dara for early Cenozoic taxa are from respective papers: *Protungulatum* (Orliac and O'Leary, 2016); *Hyopsodus* (Orliac et al., 2012a); *Diacodexis* (Orliac et al., 2012b); *Alcidedorbignya* (Muizon et al., 2015); Litopterns (Billet et al., 2015).

Species	Low-Frequency Limit (kHz)	High-Frequency Limit (kHz)
Homo sapiens (Human)	0.07	29.25
Litopterns (21.16mm)	0.08	33.7
Orycteropus afer (Aardvark)	0.21	35.19
Litopterns (16.55mm)	0.14	36.19
Alcidedorbignya	0.56	36.76
Sus scrofa (Wild boar)	0.04	41.11
Carsioptychus	0.61	47.58
Felis catus (Cat)	0.08	47.98
Protungulatum	1.09	57.21
Hyopsodus	0.32	59.13
Canis familiaris (Dog)	0.11	61.3
Kulbeckia	3.01	64.57
Sylvilagus floridanus (Rabbit)	0.4	68.77
Diacodexis	0.66	72.13
Didelphis virginiana (Opossum)	0.54	77.22
Zalamdalestes	7.55	77.93
Zhelestids	2.08	80.6
Atelerix albiventris (Hedgehog)	1.6	91.95
Mus musculus (Mouse)	2.42	119.13

Table 7. Low and high-frequency limits of hearing at 60 dB in kHz (based on West's [1985]) equations) for a range of extant and extinct mammals. Two ranges for litopterns are shown, based on different petrosal specimens with different basilar membrane lengths (Billet et al., 2015). Data for extant and Mesozoic mammals are from Ekdale (2013). Dara for early Cenozoic taxa are from respective papers: *Protungulatum* (Orliac and O'Leary, 2016); *Hyopsodus* (Orliac et al., 2012a); *Diacodexis* (Orliac et al., 2012b); *Alcidedorbignya* (Muizon et al., 2015); Litopterns (Billet et al., 2015).

Species	ASC Agility Score	PSC Agility Score	LSC Agility Score	SC Agility Score
Palaeopropithecus ingens (Sloth Lemur)	2.32	2.41	2.15	2.19
Sus scrofa (Wild boar)	2.54	2.65	2.43	2.43
Carsioptychus	2.49	2.64	2.99	2.55
Alcidedorbignya	2.94	3.01	3.13	2.83
Lutra lutra (Otter)	2.91	2.9	3.50	3.02
Hyopsodus	3.48	3.23	3.42	3.30
Protungulatum (226g)	3.47	3.40	3.49	3.36
Gazella bennetti (Gazelle)	3.31	3.35	3.20	3.37
Diacodexis (935g)	3.63	3.49	3.35	3.48
Protungulatum (148g)	3.70	3.62	3.74	3.63
Diacodexis (737g)	3.77	3.63	3.47	3.64
Notostylops	3.40	3.60	3.90	3.70
Diacodexis (554g)	3.93	3.81	3.62	3.84
Oryctolagus cuniculus (Rabbit)	3.69	3.53	3.91	4.05
Sciurus vulgaris (Squirrel)	4.47	4.18	4.9	4.99

Table 8. Agility scores for a range of extant and extinct mammals, including *Carsioptychus*, based on the equations of Silcox et al. (2009). Values for body mass are shown for those taxa in which more than one mass value has been calculated. Semi-circular canal measurements for extant mammals are from Spoor *et al*. (2007). Measurements for early Cenozoic taxa are from respective papers: *Protungulatum* (Orliac and O'Leary, 2016); *Hyopsodus* (Orliac et al., 2012a); *Diacodexis* (Orliac et al., 2012b); *Alcidedorbignya* (Muizon et al., 2015); *Notostylops* (Macrini et al., 2013).

Character	*C. coarctatus*	Theria	Eutheria	Unnamed clade 1	Unnamed clade 2	Placentalia	Unnamed clade 3	Notoungulata
2	0	0	0	0	0	0	0	0
3	0	0	0	0	0	0	0	0
4	0	0	0	0	0	0	0	0
5	0	0/1	0/1	0/1	1	0	0	0
6	0	0	0	0	0	0	0	0
7	2	0	0	0	1	0	0	0
8	0	0	0	0	0	0	0	0
9	0	0	0	0	0	0	0	0
10	1	1	1	1	1	1	1	1
11	1	1	1	1	1	1	1	1
12	1	0/1	0/1	0/1	0/1	0/1	0/1	1
13	1	0	0	1	1	1	1	1
14	0	0	0	0	0	0	0	0/1
21	0	0	0	0	0	0	0	0
22	0	0	0	0	0	0/1	0/1	0/1

Table 9. Phylogenetic characters relating to the inner ear, assessed in *Carsioptychus* and other mammals. Characters are from Macrini et al. (2013), and only characters that could be scored in the bony labyrinth of *Carsioptychus* are shown. The scores for *Carsioptychus* are those present in AMNH 27601; the scores for the other mammals are parsimony ancestral state reconstructions for major clades (from Macrini et al., 2013: Table 6). Unnamed clade 1 includes *Kulbeckia kulbecke* and *Zalambdalestes lechei*, unnamed clade 2 includes *Zalambdalestes lechei*, and unnamed clade 3 includes *Hyopsodus lepidus*.